

1-1-2012

Novel inhibitors of the bacterial de novo purine biosynthesis enzymes, n5-carboxyaminoimidazole ribonucleotide synthetase and mutase

Maria V. Fawaz
Wayne State University,

Follow this and additional works at: http://digitalcommons.wayne.edu/oa_theses

Recommended Citation

Fawaz, Maria V., "Novel inhibitors of the bacterial de novo purine biosynthesis enzymes, n5-carboxyaminoimidazole ribonucleotide synthetase and mutase" (2012). *Wayne State University Theses*. Paper 193.

This Open Access Thesis is brought to you for free and open access by DigitalCommons@WayneState. It has been accepted for inclusion in Wayne State University Theses by an authorized administrator of DigitalCommons@WayneState.

**NOVEL INHIBITORS OF THE BACTERIAL *DE NOVO* PURINE
BIOSYNTHESIS ENZYMES, *N*⁵-CARBOXYAMINOIMIDAZOLE
RIBONUCLEOTIDE SYNTHETASE AND MUTASE**

by

MARIA V. FAWAZ

THESIS

Submitted to the Graduate School

of Wayne State University,

Detroit, Michigan

in partial fulfillment of the requirements

for the degree of

MASTERS OF SCIENCE

2012

MAJOR: PHARMACEUTICAL SCIENCES

Approved by:

Advisor

Date

© COPYRIGHT BY

MARIA V. FAWAZ

2012

All Rights Reserved

DEDICATION

This work is dedicated to my husband Mike and my family.

Thank you for all the love, belief, and patience you have given me.

Without your support I would never get this far.

“Век живи – век учись!”

- Козьма Прутков

ACKNOWLEDGEMENTS

I would like to thank Wayne State University and The Department of Pharmaceutical Sciences for providing the research assistantship throughout my graduate studies. A special thanks to Dr. George Corcoran, the chairman of the department, for his tremendous support during difficult times.

I am very thankful to my committee members, Dr. David Oupicky and Dr. Sarah Trimpin whose encouragement, counsel, and constructive criticism made this thesis stronger.

Last but not least, I would like to show gratitude to my former laboratory members, Dr. Melissa Topper and Dr. Shiv Sharma. Your friendship, guidance and scientific expertise made my thesis possible.

TABLE OF CONTENTS

Dedication.....	ii
Acknowledgements.....	iii
List of Tables.....	vi
List of Figures.....	vii
List of Schemes.....	ix
List of Abbreviations.....	x
CHAPTER 1: Introduction.....	1
1.1 Antibiotic Resistance and Current Issues in Drug Discovery.....	1
1.2 Overview of the <i>de novo</i> purine biosynthesis pathway.....	4
1.3 N^5 -CAIR synthetase (PurK) and N^5 -CAIR mutase (PurE class I).....	6
1.4 De novo purine biosynthesis as antibacterial target.....	9
CHAPTER 2: Small Molecules Targeting Bacterial N^5 -CAIR Synthetase.....	10
2.1 Introduction.....	10
2.2 Results.....	14
2.2.1 Validation Study of Isatin-Based Derivatives.....	14
2.2.2 Kinetic Analysis of 7-Bromoisatin.....	15
2.3 Discussion.....	19
2.4 Materials and Methods.....	23
2.4.1 Inhibitory activity of <i>E. coli</i> N^5 -CAIR synthetase isatin-based derivatives in the pyruvate kinase/lactate dehydrogenase-coupled assay.....	23
2.4.2 Kinetic analysis of 7-bromoisatin against <i>E. coli</i> N^5 -CAIR Synthetase.....	23
2.4.3 Synthesis of 5-aminoimidazole ribonucleotide (AIR).....	25
2.4.4 Preparation of diisopropylethylammonium acetate (DIPEAA).....	25

CHAPTER 3: Small Molecules Targeting Bacterial N^5 -CAIR Mutase.....	27
3.1 Introduction.....	27
3.2 Results.....	30
3.2.1 High-throughput Screening.....	30
3.2.2 Kinetic Analysis of “Hit” Compounds.....	33
3.2.3 Molecular Modeling Study of Compound 1.....	34
3.2.4 Exploratory Synthesis of the Pure Enantiomers of 1.....	40
3.3 Discussion.....	45
3.4 Materials and Methods.....	49
3.4.1 High-throughput screening.....	49
3.4.2 Purification of Human AIR Carboxylase.....	50
3.4.3 Kinetic Analysis of Inhibitor 1.....	51
3.4.4 Molecular Modeling Study.....	52
3.4.5 Exploratory Synthesis of Compound 1.....	53
3.4.6 Optical rotation of compounds 11, 12 and 13.....	57
References.....	59
Abstract.....	70
Autobiographical Statement.....	72

LIST OF TABLES

Table 2.1.1	Inhibitory activity of isatin-based compounds in malachite green/ phosphor molybdate assay.....	12
Table 2.2.1	Inhibitory activity of isatin-based compounds evaluated using enzyme- coupled UV assay.....	15
Table 3.2.1	HTS-derived inhibitors of <i>E. coli</i> N ⁵ -CAIR mutase and human AIR Carboxylase.....	32
Table 3.4.1	Optical rotation data for L-isomers of compounds 11, 12, and 13.....	58

LIST OF FIGURES

Figure 1.1	Novel classes of antibiotics introduced into clinic from 1930 to 2012.....	4
Figure 1.2	Purine biosynthetic pathway.....	5
Figure 1.3	Divergence in the sixth step of the <i>de novo</i> purine biosynthesis pathway...8	
Figure 2.1.1	Isatin inhibitors of N^5 -CAIR synthetase.....	11
Figure 2.1.2	Discontinuous malachite green/phosphomolybdate UV assay.....	13
Figure 2.2.1	Pyruvate kinase/lactate dehydrogenase-coupled assay.....	14
Figure 2.2.2	Structure of 7-bromoisatin.....	15
Figure 2.2.3	Lineweaver-Burke plots for the inhibition of <i>E. coli</i> N^5 -CAIR synthetase by 7-bromoisatin.....	17
Figure 2.3.1	Assay comparison diagram.....	20
Figure 2.3.2	Structure of sorafenib.....	21
Figure 3.1.1	Reactions catalyzed by AIR carboxylase, N^5 -CAIR synthetase, and N^5 - CAIR mutase.....	27
Figure 3.1.2	Comparison of two monomers: human AIR carboxylase and <i>E. coli</i> N^5 - CAIR mutase.....	28
Figure 3.2.1	Enzyme-catalyzed CAIR decarboxylation assay.....	30
Figure 3.2.2	HTS flow chart.....	31
Figure 3.2.3	Lineweaver-Burke plot for the inhibition of <i>E. coli</i> N^5 -CAIR mutase.....	33
Figure 3.2.4	Structure of NAIR.....	34
Figure 3.2.5	Structures of (S) and (R) enantiomers of compound 1.....	35
Figure 3.2.6	Interaction diagram of the (S)-isomer of compound 1 docked to <i>E. coli</i> N^5 - CAIR mutase active site.....	36
Figure 3.2.7	The surface representation of <i>E. coli</i> N^5 -CAIR mutase active site with (S) enantiomer of 1.....	37
Figure 3.2.8	Interaction diagram of (R) isomer of compound 1 docked to <i>E. coli</i> N^5 - CAIR mutase active site.....	37

Figure 3.2.9	The surface representation of <i>E. coli</i> N^5 -CAIR mutase active site with (<i>R</i>) enantiomer of 1.....	38
Figure 3.2.10	Interaction diagram of (<i>S</i>) isomer of compound 1 docked to human AIR carboxylase active site.....	38
Figure 3.2.11	The surface representation of human AIR carboxylase active site with (<i>S</i>) enantiomer of 1.....	39
Figure 3.2.12	Interaction diagram of (<i>R</i>) isomer of compound 1 docked to human AIR carboxylase active site.....	39

LIST OF SCHEMES

Scheme 1	Proposed mechanism of PurK catalysis.....	8
Scheme 3.1	Retrosynthetic analysis for the synthesis of compound 1.....	41
Scheme 3.2	Synthesis of Boc- α -amino- <i>N</i> -phenylsuccinimide 12 and α -amino- <i>N</i> -phenylsuccinimide·HCl 13.....	42
Scheme 3.3	Synthesis of compound 15.....	42
Scheme 3.4	Direct <i>N</i> -alkylation reaction of 13 with 15.....	43
Scheme 3.5	Synthetic approach for the synthesis of compound 1 using 4-nitrobenzenesulfonyl chloride as protective agent.....	44

LIST OF ABBREVIATIONS

ATP	Adenosine triphosphate
PurF	Amidophosphoribosyltransferase
AICAR	Aminoimidazole-4-carboxamide ribonucleotide
PurH	5-Aminoimidazole-4-carboxamide ribonucleotide (AICAR) transformylase
AIR	5-Aminoimidazole ribonucleotide
PurM	Aminoimidazole ribonucleotide (AIR) synthetase
PurE	Aminoimidazole ribonucleotide (AIR) carboxylase (Class II)
NH ₃	Ammonia
Å	Angstrom
Boc	<i>tert</i> -Butoxycarbonyl
CO ₂	Carbon dioxide
CAIR	4-Carboxy-5-aminoimidazole ribonucleotide
N ⁵ -CAIR	N ⁵ -Carboxyaminoimidazole ribonucleotide
PurE	N ⁵ -Carboxyaminoimidazole ribonucleotide (N ⁵ -CAIR) mutase (Class I)
PurK	N ⁵ -Carboxyaminoimidazole ribonucleotide (N ⁵ -CAIR) synthetase
CCG	Center for Chemical Genomics
Cs ₂ CO ₃	Cesium carbonate
δ	Chemical shift
Da	Dalton
°C	Degrees Celsius
DNA	Deoxyribonucleic acid
DCM	Dichloromethane
NADH	Dihyronicotinamide adenine dinucleotide
DIEA	Diisopropylethylamine

DMF	<i>N,N</i> -Dimethylformamide
DMSO	Dimethylsulfoxide
d	Doublet
eq	Equivalent
PurP	Flavin 5-aminoimidazole-4-carboxamide ribonucleotide (AICAR) synthetase (prokaryotic)
FAICAR	5-Formamido-4-imidazolecarboxamide ribonucleotide
FGAR	N-Formylglycinamide ribonucleotide
FGAM	N- Formylglycinamidine ribonucleotide
PurT	Formylglycinamide ribonucleotide (FGAR) synthetase (prokaryotic)
PurL	Formylglycinamidine ribonucleotide (FGAR) synthetase
GAR	Glycinamide ribonucleotide
PurD	Glycinamide ribonucleotide (GAR) synthetase
PurN	Glycinamide ribonucleotide (GAR) transformylase
g	Gram
IC ₅₀	Half maximal inhibitory concentration
HPLC	High-performance liquid chromatography
HTS	High-throughput screening
h	Hour
HCl	Hydrochloric acid
HEPES	N-(2-Hydroxyethyl)-piperazine-N-(2-ethanesulfonic acid)
K _i	Inhibition constant
IMP	Inosine monophosphate
PurJ	Inosine monophosphate (IMP) cyclohydrolase
PurO	Inosine monophosphate (IMP) cyclohydrolase (prokaryotic)

MRSA	Methicillin resistant <i>Staphylococcus aureus</i>
μM	Micromolar
mL	Milliliter
mM	Millimolar
MOE	Molecular Operating Environment
m	Multiplet
ng	Nanogram
nM	Nanomolar
PRPP	5-Phosphoribosylpyrophosphate
PRA	5-Phospho-D-ribosylamine
TMSOK	Potassium trimethylsilanolate
PDB	Protein Data Bank
¹ H NMR	Proton Nuclear Magnetic Resonance
RNA	Ribonucleic acid
RT	Room temperature
PurB	SAICAR lyase
s	Singlet
SAICAR	Succino 5-aminoimidazole-4-carboxamide ribonucleotide
PurC	N- Succinyl 5-aminoimidazolyl-4-carboxamide ribonucleotide synthetase
TBAI	Tetrabutylammonium iodide
THF	Tetrahydrofuran
t	Triplet
Tris	Tris-(hydroxymethyl)aminomethane
UV	Ultraviolet
VRE	Vancomycin-resistant <i>Enterococcus faecium</i>

CHAPTER 1

INTRODUCTION

1.1 Antibiotic Resistance and Current Issues in Drug Discovery

The discovery of the first commercially available antibiotic, penicillin, in 1928 has proven to be one of the greatest achievements of the 20th century (1). Antibiotics have saved millions of lives around the globe by reducing human mortality and revolutionizing medicine in many aspects (2). The availability of antimicrobial agents allows treatment of otherwise deadly infections such as syphilis, pneumonia, and rheumatic fever. In addition, major invasive surgeries as well as chemotherapy are now possible and have achieved high success rates (3).

More than 80 years have passed since Alexander Fleming discovered penicillin, leading to a vast increase in the antimicrobial drug research (4). While hundreds of antibiotics have been introduced into the clinic since then, these agents typically function on a very limited number of microbial targets (5). Antimicrobial agents predominantly target DNA and RNA synthesis (e.g., fluoroquinolones), cell wall biosynthesis (e.g., β -lactams), cell membrane (e.g., daptomycins) construction, protein synthesis (e.g., tetracyclins), or folic acid metabolism (e.g., sulfonamides) (6). The relatively limited set of targets, coupled with other mechanisms discussed below, have led to a decrease in the effectiveness of antibiotics (2, 7).

The intensive use of antibiotics results in the remarkable increase of the bacterial resistance (3). One example of how fast bacteria are able to develop resistance to a new therapy can be demonstrated by the archetypical human pathogen called tuberculosis (TB). Currently, this bacteria infects almost one-third of the world's population (1). Highly effective anti-TB antibiotics such as streptomycin and isoniazid were introduced into clinic in the late 1940s and resulted in the saving of millions of lives. However, bacteria

have developed resistance to these drugs (8). Nowadays, treatment of TB infections is difficult due to inappropriate use of previously effective antibiotics. The new anti-TB drug regimen consists of a cocktail of multiple anti-infective agents (1). Recently, another dangerous human pathogen, *Pseudomonas aeruginosa*, became a major health threat. *P. aeruginosa* was historically associated with burn wounds, but has now become a serious hospital-acquired pathogen (9). This bacterium has traditionally been treated with β -lactams and aminoglycosides, however the ineffectiveness of these drugs against *P. aeruginosa* has led to the clinical introduction of more potent antibiotics such as quinolones and lipopeptides (10). In recent years, *Staphylococcus aureus* has rapidly evolved as a drug-resistant “superbug” (11). Until the 1960s, *S. aureus* was manageable with penicillin. Yet, three years after penicillin analog, methicillin, was introduced into the clinic, methicillin-resistant strains of *S. aureus* were detected. Currently, 60% of *Staphylococcal* infections are resistant to at least one antibiotic (12).

While antibiotic resistance has been presented in the media as a new medical problem, resistance has always been observed (7). Generally, microbial resistance occurs via immunity bypass, enzyme-catalyzed destruction of the antibiotic, efflux of the drug from the bacterial cell or modification of the target so that the antibiotic no longer binds. One alarming issue with bacterial resistance is the fact that bacteria can transfer resistance genes to both their progeny and also other bacteria in the environment (3).

The growing concern regarding antibiotic resistance in the 1990s has primarily been focused on the Gram-positive bacterial pathogens including methicillin-resistant *S. aureus* (MRSA), vancomycin-resistant *Enterococcus faecium* (VRE), and penicillin-resistant *S. pneumoniae* (13). However, antibiotics are urgently needed for Gram-negative bacterial strains to treat pan-antibiotic-resistant *Acinetobacter baumannii*, carbapenem-resistant *Klebsiella pneumoniae*, and fluoroquinolone-resistant *P.*

aeruginosa and *Enterobacter* species (13, 14). The issue of antibacterial resistance is heightened by the fact that over the past 30 years, only two novel classes of antibiotics (oxazolidinone-linezolid and lipopeptide-daptomycin) have been introduced into the clinic (Figure 1.1) (14). Unfortunately, this fact is unlikely to be changed in the near future. Currently, there are 150 antibacterials in preclinical development, but only 7 are in Phase III clinical trials. Although there is a growing need for new drugs, the antibiotic market has shown only a 4% increase over the last 5 years (13). Those numbers are extremely low and need a drastic turn-around; however, fierce economic pressures associated with developing a new antiinfective agent (~10 years and \$800M) coupled with the high rates of resistance shortly after introduction into clinic continue to challenge the field (15).

Clearly, there is a growing need for new antibiotics with novel mechanisms of action (14). Traditionally, antimicrobial agents have been either natural products or their derivatives (16). However, there is a wide array of resistance mechanisms incorporated into the bacterial genome for many natural products, limiting some of their utility in the field of drug discovery. This has suggested to researchers that new approaches focused more on the synthetic drug development are required (3). High-throughput screening (HTS) is one method that might offer additional advantages to the antibiotic drug discovery due to its unbiased nature and the fact that extensive libraries of compounds (>1,000,000) are available.

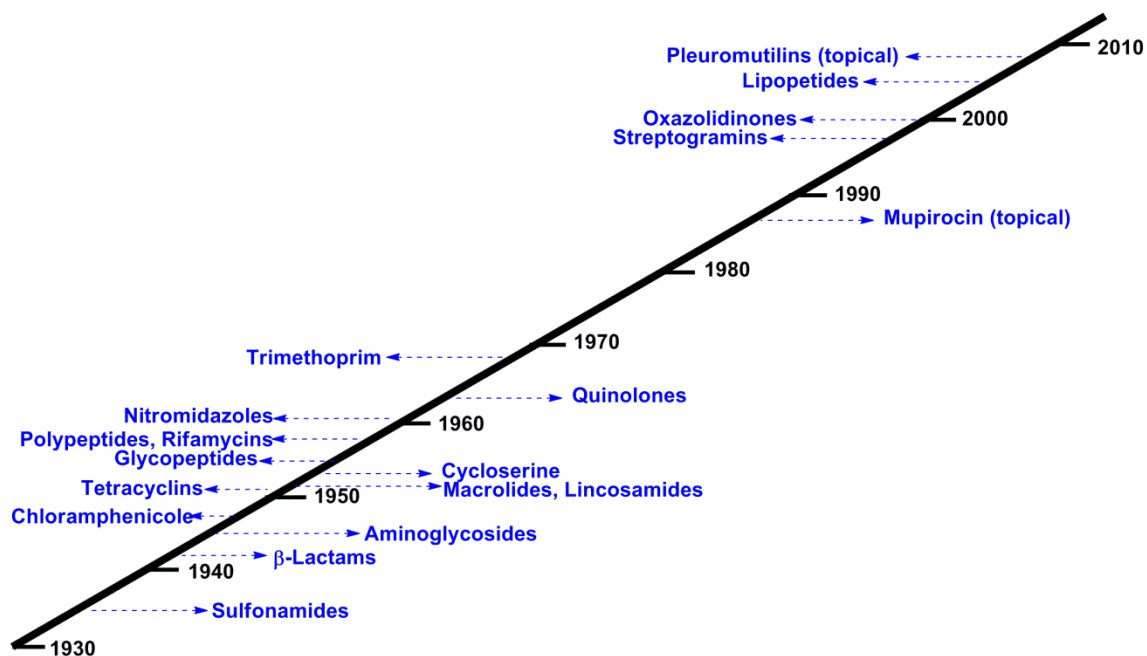


Figure 1.1 Novel classes of antibiotics introduced into clinic from 1930 to 2012.

One promising area of antimicrobial drug discovery is the *de novo* purine biosynthesis pathway (17). In the 1980s, a divergence was found between the bacterial and human purine biosynthesis pathways. The pathway in bacteria requires 11 steps to synthesize inosine monophosphate (IMP) and involves two additional enzymes, both of which are absent in humans (18). These differences between bacterial and human *de novo* purine biosynthesis make this pathway an ideal target for the antibiotic drug research.

1.2 Overview of the *de novo* purine biosynthesis pathway

Adenylate and guanylate are required for numerous key biological processes, including the synthesis of DNA and RNA, chemical energy, and as parts of other important biomolecules (e.g. NADH, coenzyme A, etc.) (19). There are two pathways for the synthesis of these nucleotides. The first is the *de novo* purine biosynthetic pathway. This pathway was elucidated in the 1950s by Buchanan *et al.* who showed that

phosphoribosyl pyrophosphate (PRPP) is converted into inosine monophosphate (IMP) via a 10-step enzymatic process in higher eukaryotes (Figure 1.2) (20, 21). IMP is formed from small molecule precursors including glycine, glutamine, aspartate, carbon dioxide, N¹⁰-formyl-tetrahydrofolate, and ribose-5-phosphate which build-up the purine heterocycle onto the sugar (20). Once IMP is formed, IMP can be converted into either adenosine monophosphate (AMP) or guanosine monophosphate (GMP) depending upon the needs of the cell. The second pathway for purine synthesis is the salvage pathway which recycles purine bases generated during metabolic degradation of nucleotides. However, this pathway produces only 1% or less of the total nucleotides needed for DNA synthesis (22). Therefore, *de novo* purine biosynthesis is the major process for generating purine bases needed for replication of organisms.

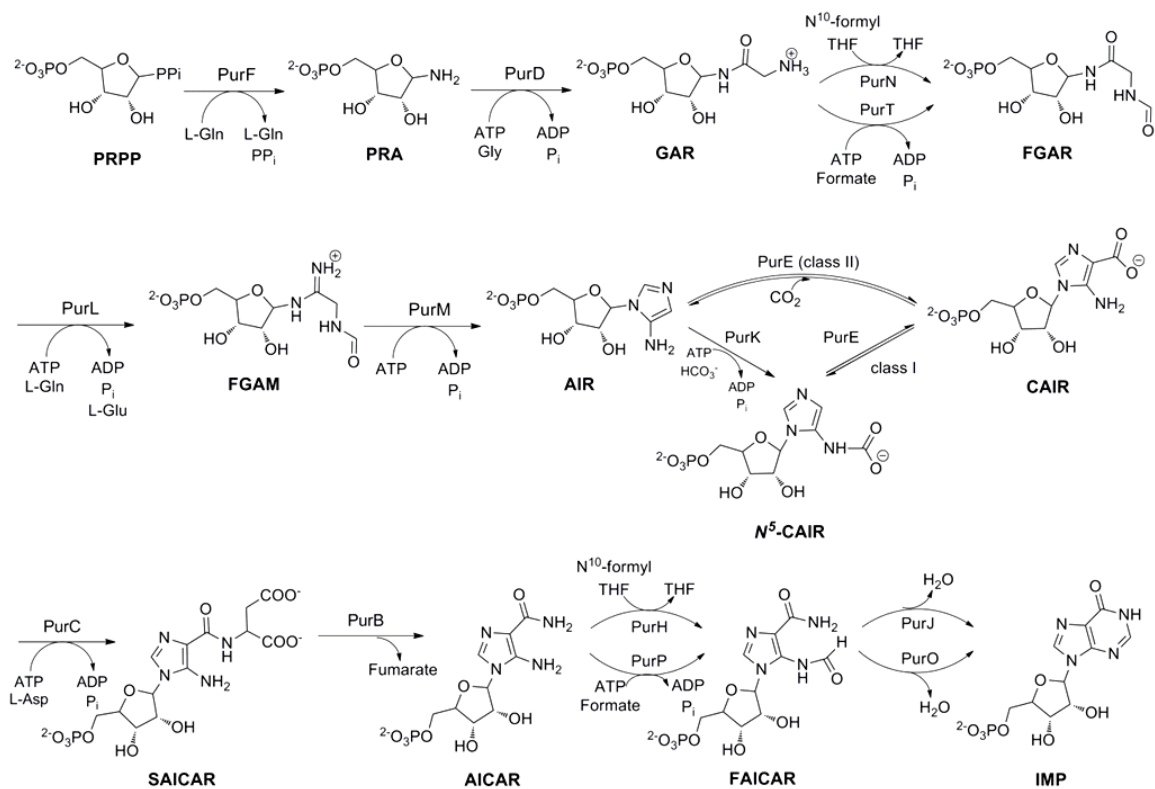


Figure 1.2 Purine biosynthetic pathway (20). Enzyme names in the diagram are presented by their designated genes.

The pathway elucidated by Buchannan remained essentially unchanged until research in the 1990s showed that there were differences in the pathway between higher eukaryotes (e.g., humans) and bacterial, yeast and fungi. Research on the pathway noted that enzymes such as PurF, PurD, PurL, PurM, and PurB were ubiquitous while PurN or PurT, PurK/PurE (class I) or PurE (class II), PurH or PurP, and PurJ or PurO varied between organisms (Refer to the List of Abbreviations on page viii) (20). Differences in the *de novo* purine biosynthetic pathway were found not only at the protein level, but also in the gene organization where it was common for higher organisms to have fused gene products (e.g., human PAICS with PurC and PurE class II subunits). It was previously postulated that the fusion of several enzymes might be important for substrate channeling (23).

Despite multiple differences, several enzymes in the pathway use the same mechanistic strategies and have a high structural homology suggesting a convergent evolutionary origin (20). These enzymes include PurP, PurK, PurT, and PurD, all of which catalyze a coupling reaction of an amino group with a carboxylate group via a formation of an acylphosphate intermediate (20). These enzymes belong to the ATP-grasp superfamily (24, 25). In addition to the above-mentioned enzymes, Class I and II PurEs are also structurally and functionally related to each other.

1.3 N^5 -CAIR synthetase (PurK) and N^5 -CAIR mutase (PurE class I)

The sixth step in *de novo* purine biosynthesis is the only carbon-carbon bond forming reaction in the pathway. PurE is the enzyme that catalyzes this unique chemical transformation which transforms aminoimidazole ribonucleotide (AIR) to 4-carboxy-5-aminoimidazole ribonucleotide (CAIR) with the aid of CO₂. For about 30 years, the PurE enzyme was thought to be the same in all organisms and was universally called AIR carboxylase. However, in the early 1990s, researchers showed that in bacteria, yeast

and fungi, two enzymes were required to convert AIR to CAIR (Figure 1.3). This discovery was initiated by attempting to identify the AIR carboxylase gene in microbes. Zengado *et al.* and Watanabe *et al.* identified two different genes within the PurE locus (PurK and PurE) (26). Later, Zalkin *et al.* reported a 429 amino acid protein using chicken liver cDNA that was similar to the bacterial PurE protein, but did not possess any protein analogous to PurK (27). A key question remained: why are there two genes for the conversion of AIR to CAIR in microorganisms? To address this question and establish the function of PurK, Stubbe *et al.* purified both the PurK and PurE protein (28). These researchers discovered that PurE was capable of converting AIR into CAIR; however, only in the presence of non-physiological concentrations of bicarbonate. The addition of PurK and ATP led to a rapid production of CAIR under conditions with low concentrations of bicarbonate. These studies indicated that PurK appeared to act as a CO₂ generation system for PurE. Additional studies revealed that PurK synthesized the short-lived intermediate, N⁵-CAIR from AIR and PurE converted N⁵-CAIR into CAIR (29). Thus, PurK was named N⁵-CAIR synthetase while PurE (Class I) was renamed N⁵-CAIR mutase. Studies on N⁵-CAIR synthetase indicated that the reaction took place via a formation of a carboxyphosphate intermediate that dissociated to give carbon dioxide (CO₂). Subsequently, CO₂ was attacked by AIR to produce N⁵-CAIR (Scheme 1).

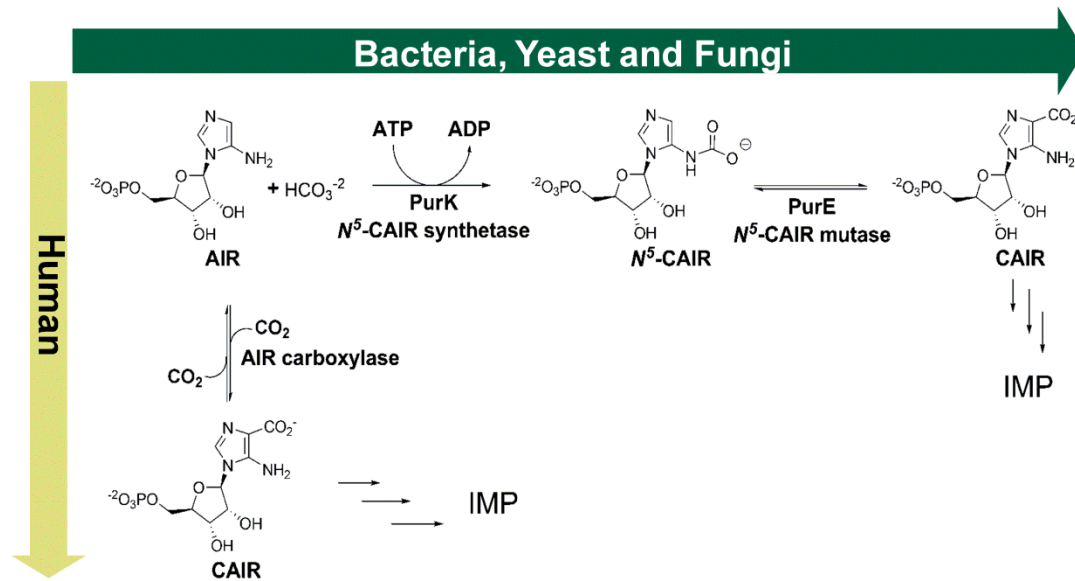
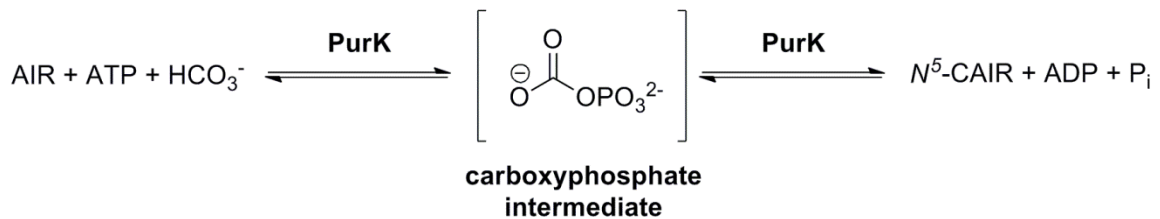


Figure 1.3 Divergence in the sixth step of the *de novo* purine biosynthesis pathway (30).

Scheme 1 Proposed mechanism of PurK catalysis (30).



The discovery of a new intermediate in *de novo* purine biosynthesis prompted an examination of the pathway in higher eukaryotes. As mentioned above, work by Zalkin and colleagues revealed that higher eukaryotes lacked a PurK gene. This suggested that the pathway in higher eukaryotes was different. To verify this, studies were conducted using the enzyme from chicken. This research revealed that in higher eukaryotes AIR and CO₂ directly converted to CAIR. Thus, the protein is AIR carboxylase enzyme.

1.4 De novo purine biosynthesis as antibacterial target

The divergence, described above, provide a significant biochemical rationale for investigating *de novo* purine biosynthesis as an antibacterial drug target. This contention has also been supported by genetic and medical studies on purine auxotrophs. These studies have shown that the purine biosynthetic pathway is important for the bacterial virulence once a microorganism is inside the host (31). It has been shown that bacterial strains auxotrophic for purines are significantly less virulent than the wild-type strains (32, 33). The study conducted by Perfect *et al.* on *Cryptococcus neoformans* *ade2* auxotrophs (the same gene as PurK/PurE) showed that they were unable to replicate in a meningitis animal model while complemented strains demonstrated a restored virulence (34). *Shigella flexneri* PurE and PurK mutants exhibited no virulence and impaired bacterial growth in animal models (35). Other researchers have also shown a dependence of microbial virulence on the presence of PurK and PurE genes (36-38). Together, these studies validate the hypothesis that N^5 -CAIR synthetase (PurK) and N^5 -CAIR mutase (PurE) are targets for the development of new antibiotics.

In this thesis, the discovery and biological evaluation of unique classes of inhibitors targeting bacterial N^5 -CAIR synthetase and N^5 -CAIR mutase enzymes will be presented.

CHAPTER 2

SMALL MOLECULES TARGETING N^5 -CAIR SYNTHETASE

2.1 Introduction

N^5 -CAIR synthetase is a unique enzyme present in bacteria, yeast and fungi, but not in humans (18, 39). Studies on this enzyme have shown that it plays an important role in microbial growth and disease progression (40). Deletion of the N^5 -CAIR synthetase gene produces a non-virulent strain of bacteria that is incapable of propagating in human or mouse serum (33, 34, 37, 38, 41-43). These results agree with recent work by Lan *et al.* (2010) who has shown that 6-thioguanine can inhibit *de novo* purine biosynthesis and, as a result, suppress the virulence of *S. aureus* (36). This evidence validates N^5 -CAIR synthetase as an ideal target for the discovery of inhibitors targeting *de novo* purine biosynthesis in bacteria. Given the current challenges of commercially available antibiotics, antibacterial agents with novel mechanisms of action will be invaluable against the growing problem of the bacterial resistance (3, 16).

While there had been ample evidence for targeting N^5 -CAIR synthetase, there were no known small-molecule inhibitors of N^5 -CAIR synthetase before a publication by our laboratory in 2009 (17). This publication outlined a HTS study conducted at the Center for Chemical Genomics (CCG) at the University of Michigan to identify drug-like inhibitors of N^5 -CAIR synthetase. The study identified 14 inhibitors (hit rate: 0.03%) with IC_{50} values below 70 μ M (17). All compounds followed the Lipinski's rules (44). Out of 14 initial "hits", 6 had an isatin (1H-indole-2,3-dione) core (Figures 2.1.1 a and c). The isatin class of inhibitors was potent against bacterial N^5 -CAIR synthetase (IC_{50} (HTS) ranging from 2.3 to 69 μ M). The Michaelis-Menten studies of one of the isatin inhibitors showed non-competitive kinetics with respect to ATP and AIR suggesting the possibility of a unique binding pocket on N^5 -CAIR synthetase (17).

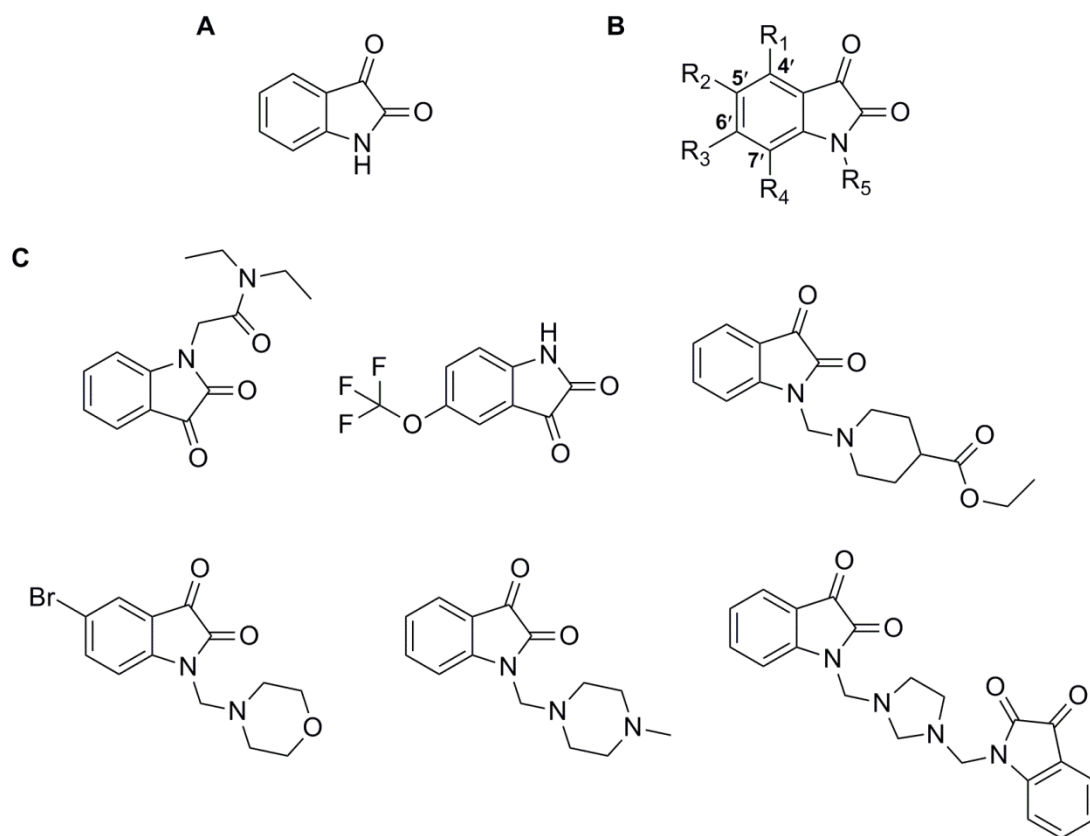


Figure 2.1.1 Isatin inhibitors of N^5 -CAIR synthetase. (A) The isatin core structure; (B) Isatin nomenclature; (C) Isatin-based inhibitors discovered from HTS.

To improve the potency of isatin inhibitors, researchers in our laboratory initiated an extensive study focused on the multiple substitutions and modifications of the core isatin structure. From these studies, initial structural-activity relationships (SAR) could be deduced (Table 2.1.1). It was found that the inhibitory effects of isatin-derivatives varied depending on the structural modification of the isatin core. Introduction of electron-withdrawing groups (e.g. halogenation and nitrosation) at the 5', 6', and 7' positions resulted in a substantial increase in inhibition. Small substitutions on the nitrogen also lead to an increase in potency.

Table 2.1.1 Inhibitory activity of isatin-based compounds (see Figure 2.1.1 for nomenclature) in the malachite green/phosphomolybdate assay (Unpublished results).

Biological evaluation was performed by Dr. Melissa Topper.

Compound	R₁	R₂	R₃	R₄	R₅	IC₅₀, μM
1	Cl	H	H	H	H	75 ± 2
2	H	Cl	H	H	H	10.0 ± 0.8
3	H	H	H	Cl	H	7.6 ± 2.0
4	H	F	H	H	H	10.5 ± 0.8
5	H	H	F	H	H	35 ± 5.3
6	H	H	H	F	H	5.6 ± 4.5
7	H	NO ₂	H	H	H	4.6 ± 0.7
8	H	OCH ₃	H	H	H	15 ± 2.1
9	H	I	H	H	H	17 ± 3.4
10	H	CH ₃	H	H	H	18 ± 3.3
11	H	SO ₃ Na	H	H	H	12.5 ± 2.8
12	H	OCF ₃	H	H	H	8.0 ± 1.5
13	H	H	H	OCH ₃	H	25.3 ± 3.6
14	H	Br	Br	H	H	5.0 ± 0.4
15	H	Br	H	Br	H	7.4 ± 2.1
16	H	Br	Br	Br	H	6.8 ± 1.2
17	H	Cl	H	Cl	H	4.5 ± 0.8
18	H	Br	H	H	CH ₃	4.6 ± 2.5
19	H	Br	H	Br	CH ₃	4.2 ± 0.6
20	H	Br	H	NO ₂	H	6.9 ± 0.9
21	H	NO ₂	H	Br	H	8.7 ± 3.5
22	H	Br	H	NO ₂	CH ₃	3.8 ± 0.3
23	H	NO ₂	H	Br	CH ₃	3.9 ± 0.6

The data presented in the Table 2.1.1 was generated using the malachite green assay which measured phosphate, a product of the reaction. This assay was optimized by Firestine *et al.* to be used primarily in the HTS study (Figure 2.1.2) (17). While the assay is fast and robust, it suffers from several drawbacks. First, it is very sensitive to phosphate, which is a common contaminant in water and glassware. This can lead to a large background signal. Second, the assay is discontinuous meaning that the reaction must be manually stopped before the UV measurement is taken. This introduces error in the time of the reaction, which in turn, affects the kinetics measured by this assay. Finally, because the assay measures phosphate, it is subjected to the phosphate release kinetics of the enzyme. Thus, compounds which alter the release kinetics of phosphate but do not alter the catalysis of the enzyme would result in an aberrant K_i value. Since the determination of the kinetic mechanism of the isatin inhibitors was the primary interest, the discontinuous nature of the phosphate assay precluded its use. Given this problem, along with the other issues listed above, an examination of a second assay was necessary to establish the validity of the IC_{50} values for the isatin-based derivatives. In this chapter, the pyruvate kinase/lactate dehydrogenase-coupled UV assay system (Figure 2.2.1) is examined to present a comparison with the IC_{50} values determined from the phosphate assay (30). In addition, the kinetics and the mode of inhibition of one representative isatin-based, 7-bromoisatin, are presented.

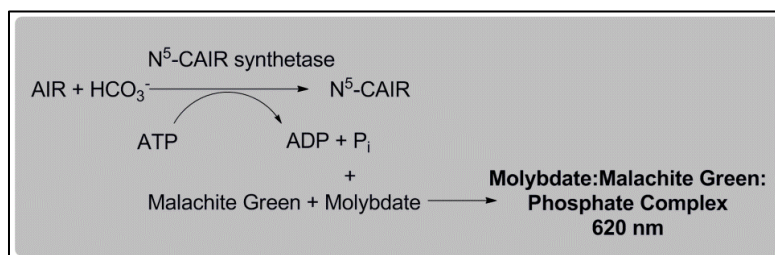


Figure 2.1.2 Discontinuous malachite green/phosphomolybdate UV assay.

2.2 Results

2.2.1 Validation Study of Isatin-Based Derivatives

The pyruvate kinase/lactate dehydrogenase-coupled assay (Figure 2.2.1), used to determine the IC_{50} values for the isatin derivatives, has been well established for N^5 -CAIR synthetase (29). This assay measures the oxidation of NADH at 340 nm as a function of the ADP produced by N^5 -CAIR synthetase during its conversion of AIR into N^5 -CAIR. The pyruvate kinase/lactate dehydrogenase-coupled assay is continuous which makes it ideal for determining the kinetics of isatin inhibitors.

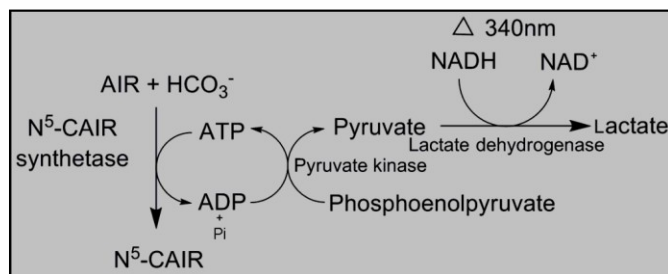


Figure 2.2.1 Pyruvate kinase/lactate dehydrogenase-coupled assay (30).

To study the correlation in IC_{50} parameters between the malachite green/phosphomolybdate and pyruvate kinase/lactate dehydrogenase-coupled assays, six representative isatin compounds with high, intermediate, and low IC_{50} values were chosen. Among these isatin derivatives were 4-chloroisatin (**1**), 7-chloroisatin (**3**), 6-fluoroisatin (**5**), 5-methoxyisatin (**8**), 7-methoxyisatin (**13**), and 5,7-dibromoisatin (**15**). Given the distinct differences in the assay components as well as the variations in the enzyme and substrate concentrations used in each assay, direct comparison of IC_{50} 's could not be performed. However, the correlation between malachite green and enzyme-coupled assays could still be evaluated based on the trend of their IC_{50} 's (Table 2.2.1). It was found that the assays were highly consistent. Compounds **3** and **15** displayed the

highest potency in both assays while inhibitors **8** and **13** showed moderate activity and compounds **1** and **5** were the least potent inhibitors of N^5 -CAIR synthetase.

Table 2.2.1 Inhibitory activity of isatin-based compounds evaluated using both the phosphomolybdate and coupled assay systems.

Compound	IC ₅₀	IC ₅₀
	Enzyme-coupled Assay, μM	Malachite Green assay, μM
15	15 \pm 2.2	7.4 \pm 2.1
3	37.5 \pm 2.6	7.6 \pm 2.0
8	59 \pm 2.7	15 \pm 2.1
13	76.8 \pm 4	25.3 \pm 3.6
5	87 \pm 2.8	35 \pm 5.3
1	153 \pm 12	75 \pm 2

2.2.2 Kinetic Analysis of 7-Bromoisatin

While the structure of N^5 -CAIR synthetase from a number of organisms (e.g. *E. coli*, *S. aureus*, and *T. thermophilus*) has been solved, the structure of isatin analogs bound to the enzyme haven't been determined. This raises a key question regarding the binding location of these potent compounds. Michaelis-Menten kinetic analysis can provide valuable information about the mechanism of inhibition and by inference, the binding site of the inhibitor. To explore the kinetics of isatin derivatives, 7-bromoisatin (Figure 2.2.2) was chosen as a representative compound with a low micromolar IC₅₀ of 6.2 μM .

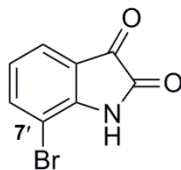
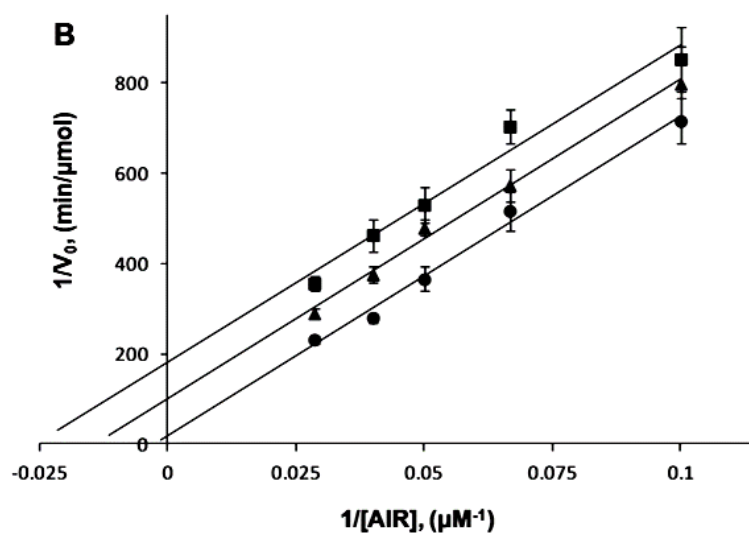
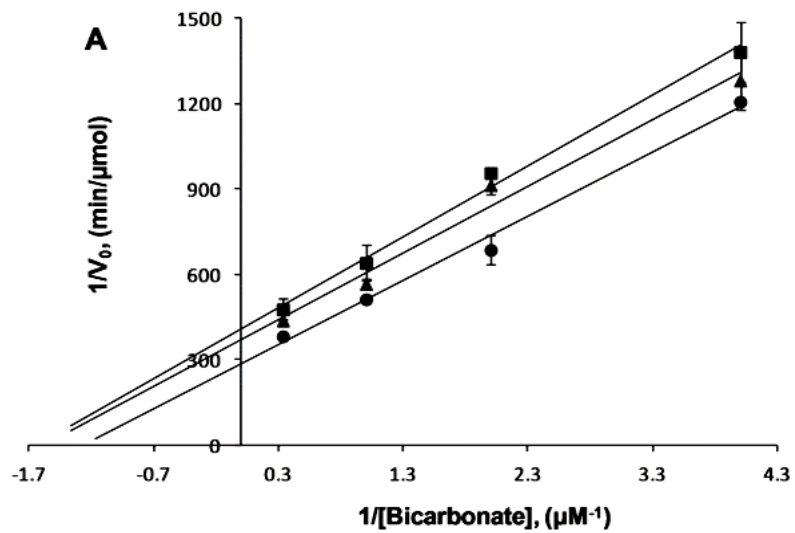


Figure 2.2.2 Structure of 7-bromoisatin.

The kinetics of 7-bromoisatin were determined by varying bicarbonate, ATP, and AIR concentrations and plotting this data against N^5 -CAIR synthetase catalyzed reaction rates to construct a series of Lineweaver-Burk plots (Figure 2.2.3). It was found that 7-bromoisatin was uncompetitive with respect to AIR (Figure 2.2.3 b) and showed mixed type of inhibition with respect to bicarbonate and ATP (Figures 2.2.3 a and 2.2.2 c).



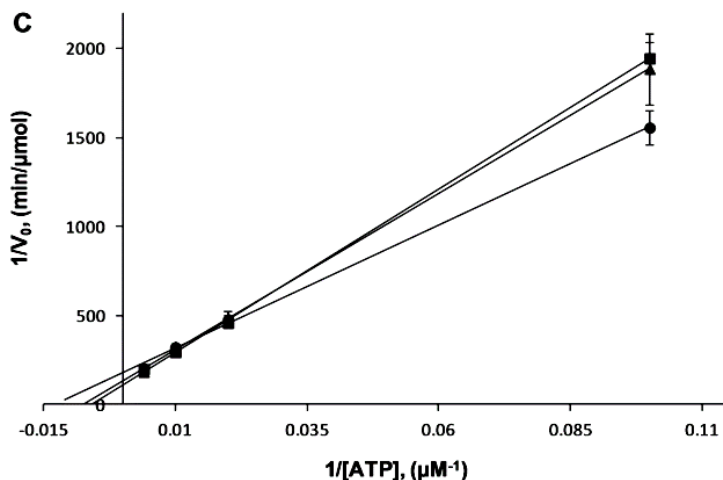


Figure 2.2.3 Lineweaver-Burke plots for the inhibition of *E. coli* N^5 -CAIR synthetase by 7-bromoisatin (**17**). (A) Lineweaver-Burke plot with varied concentration of bicarbonate, fixed concentration of ATP, AIR, and various concentrations of **17** ((●) 0 μM , (▲) 5 μM , and (■) 8 μM). (B) Lineweaver-Burke plot with varied concentration of AIR, fixed concentration of bicarbonate, AIR, and various concentrations of **17** ((●) 0 μM , (▲) 2.5 μM , and (■) 5 μM). (C) Lineweaver-Burke plot with varied concentration of ATP, fixed concentration of bicarbonate, AIR, and various concentrations of **17** ((●) 0 μM , (▲) 5 μM , and (■) 8 μM).

The uncompetitive nature of 7-bromoisatin with respect to AIR suggested that it could only bind to N^5 -CAIR synthetase in the presence of the substrate and then inhibit the enzyme. The GraphPad Prism software package was used to calculate the inhibition constant of 7-bromoisatin with respect to AIR based on its uncompetitive kinetics and it was found to be $0.71 \pm 0.47 \mu\text{M}$.

Mixed kinetics of 7-bromoisatin with respect to bicarbonate and ATP implied that the inhibitor could bind to the enzyme either in the presence or absence of these substrates. The inhibition constant was also calculated using GraphPad Prism software package for bicarbonate data. The K_i value of 7-bromoisatin with respect to bicarbonate

was $24.7 \pm 10 \mu\text{M}$. Inhibition constant of 7-bromoisatin with respect to ATP could not be generated due to ambiguity of the kinetics where GraphPad Prism software was unable to fit this data into the equations for mixed type of inhibition.

2.3 Discussion

Compounds containing isatin in their core structure have been known for more than a century (45, 46). Yet, it has only recently been acknowledged that they exhibit a range of biological activities including antiplasmodial, antiviral, anticonvulsant and many other activities (47-50). In addition, Schiff and Mannich bases of isatin display antibacterial activity (51, 52). Isatin is very abundant in nature and can be found in plants of specific genus, in frogs, and as a metabolic derivative of adrenaline in humans (46, 53, 54). The isatin derivative, sunitinib, is a receptor tyrosine kinase inhibitor that has been approved by the FDA in 2006 to treat gastrointestinal stromal tumor and renal cell carcinoma (55). All of the above mentioned properties of isatin make it a unique foundation for a wide variety of medicinal applications.

In this chapter, the inhibitory activity of six representative isatin-based compounds created by the modification of the isatin core was verified. It was found that the enzyme-coupled assay was consistent with malachite green assay since their enzyme inhibition trends were identical. Thus, compounds **3** and **15** were the most potent in both assays, while **1** and **5** were the least potent inhibitors of N^5 -CAIR synthetase (Figure 2.3.1). However, the IC_{50} values were significantly different between the assays and varied by as much as 2-4 fold from one another.

The inconsistency between the assays was expected since IC_{50} values strongly depended on the specific experimental conditions as well as the kinetic mechanism of the inhibitor (56). For example, the concentration of N^5 -CAIR synthetase was higher in the pyruvate kinase/lactate dehydrogenase-coupled compared to the malachite green/phosphomolybdate assay. Thus, more inhibitor was needed to saturate the enzyme. Despite the fact that half maximal inhibitory concentrations were different, the

second assay validated the fact that these compounds inhibited the enzyme, hence providing invaluable information for the future optimization of isatin compounds.

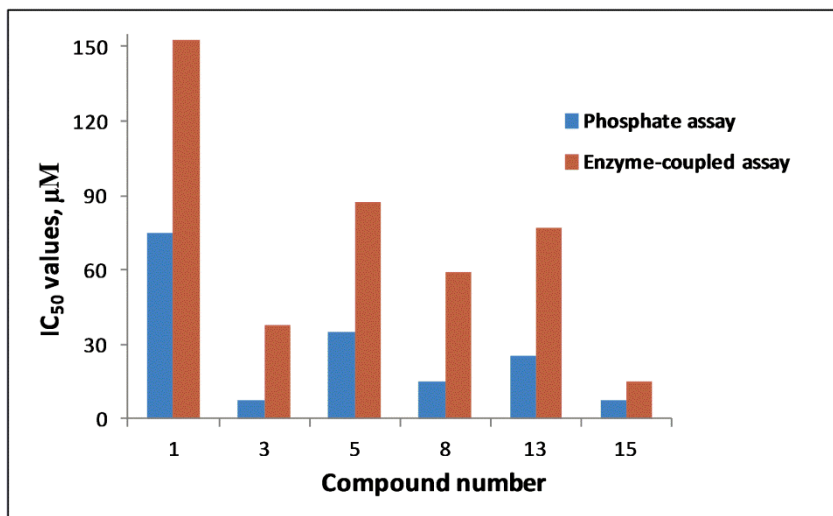


Figure 2.3.1 Comparison of the IC_{50} values obtained from the malachite green/phosphomolybdate assay (blue) and pyruvate kinase/lactate dehydrogenase-coupled assay (red).

To better understand the mechanism of N^5 -CAIR synthetase inhibition by isatins, kinetic evaluation of one representative, potent inhibitor, 7-bromoisatin, was conducted. This study utilized the continuous pyruvate kinase/lactate dehydrogenase-coupled assay. It was found that 7-bromoisatin was uncompetitive with respect to AIR ($K_i = 0.71 \pm 0.47 \mu\text{M}$) and showed mixed type of inhibition with respect to bicarbonate ($K_i = 24.7 \pm 10 \mu\text{M}$) and ATP. If 7-bromoisatin was competitive with any substrate, the location of its binding site on the enzyme would be evident. Unfortunately, 7-bromoisatin had a more complex mechanism of action. The uncompetitive nature of 7-bromoisatin inhibitor with respect to AIR indicated that it could only bind in the presence of this substrate and at a different location on the enzyme from AIR. In addition, it was possible for 7-bromoisatin to bind to the enzyme in the presence or absence of ATP and bicarbonate and inhibit the

enzyme allosterically. This type of behavior signified that 7-bromoisatin bound either somewhere outside the active site or in an active site pocket created after a conformational change was induced by substrate binding to the enzyme. Given the fact that the core structure of all compounds is isatin, it is anticipated that the same binding site identified for 7-bromoisatin is used by the rest of the inhibitors. These results are extremely important because they provide crucial information about the binding properties of the isatin-based inhibitors.

Is there precedence for an allosteric binding site in N^5 -CAIR synthetase? To date, no allosteric regulators of the enzyme have been identified. However, N^5 -CAIR synthetase is mechanistically and structurally related to the multi-subunit enzyme called acetyl-CoA carboxylase. In the mid 1990s, soraphen A (Figure 2.3.2) was found to be a nanomolar non-competitive inhibitor of one acetyl-CoA carboxylase domain called biotin carboxylase (57, 58). Later, researchers from Columbia University solved the crystal structure for soraphen A bound to the yeast biotin carboxylase domain (59). This structure revealed that soraphen A bound to a previously unrecognized allosteric site of the enzyme that was 25 Å away from its active site. In addition, the structural data showed that soraphen A could bind in the biotin carboxylase dimer interface and inhibited the enzyme by disrupting the oligomerization of this domain.

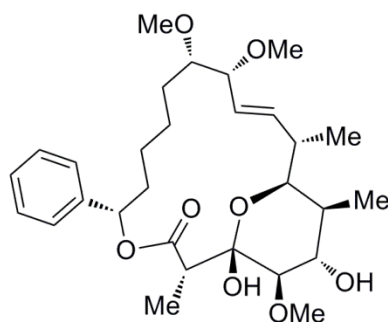


Figure 2.3.2 Structure of soraphen A.

It is quite possible that isatin compounds may also inhibit N^5 -CAIR synthetase in a manner similar to soraphen A. 7-Bromoisatin is a non- or un-competitive inhibitor with respect to the N^5 -CAIR synthetase substrates, which is typically associated with allosteric inhibitors. Also, N^5 -CAIR synthetase is a dimer (60). Therefore, the allosteric effects of 7-bromoisatin may be due to disrupting dimer formation. Clearly, there is a great need for a high-resolution crystal structure of N^5 -CAIR synthetase with a bound isatin molecule. Once structural data are available, docking studies will open the doors for the optimization of already existing isatin-based inhibitors of N^5 -CAIR synthetase which should result in improved potency.

In conclusion, the studies presented here have validated isatin analogs as inhibitors of N^5 -CAIR synthetase and have also provided kinetic information regarding their action on the enzyme. This information should help in the design of more potent compounds against microbial *de novo* purine biosynthesis and ultimately may prove useful as antibacterial drugs with a novel mechanism of action.

2.4 Materials and Methods

Analytical HPLC experiments were performed on a Waters 600 instrument using a PRP1 reversed-phase column (Hamilton). Enzymatic assays were conducted on a Varian UV-vis Cary 100 spectrophotometer equipped with a cell changer and a temperature controller.

2.4.1 Inhibitory activity of *E. coli* N⁵-CAIR synthetase isatin-based derivatives in the pyruvate kinase/lactate dehydrogenase-coupled assay

Half maximal inhibitory concentrations (IC₅₀) of compounds **1**, **3**, **5**, **8**, **13**, and **15** were determined using the procedure published by Paritala *et al.* (30) with the following modifications. The total reaction volume was 0.5 ml, each experiment was performed in duplicate, the pH of the HEPES buffer was 7.8, and the reagents were incubated for 2 min before the addition of *E. coli* N⁵-CAIR synthetase. Each compound was dissolved in DMSO and tested at various concentrations. The rate of NADH oxidation was monitored at 340 nm. The data generated was analyzed by plotting initial velocity against various inhibitor concentrations to generate a dose-response curve. These plots were analyzed using the GraphPad Prism software package. IC₅₀ values (equation 1) and their standard errors with 95% confidence intervals were generated by the GraphPad Prism software.

$$\frac{V_i}{V_0} = \frac{1}{1 + ([I]/IC_{50})^n} \quad (1),$$

where V_i is the reaction velocity at a specific inhibitor concentration $[I]$, V_0 is the uninhibited velocity, and $n=1$ is the Hill slope.

2.4.2 Kinetic analysis of 7-bromoisatin against *E. coli* N⁵-CAIR synthetase

The procedure by Firestine *et al.* (17) with several modifications was used to determine kinetics of 7-bromoisatin. The total reaction volume was 0.5 ml, each experiment was performed in duplicate, the pH of the HEPES buffer was 7.8, and the

reagents were incubated for 2 min before the addition of *E. coli* N^5 -CAIR synthetase. Compound 7-bromoisatin was dissolved in DMSO and tested at 2.5, 5 and 8 μ M concentrations. For the experiments in which ATP (1.0 mM) and AIR (10 μ M) were held constant, concentrations of NaHCO_3 were varied from 0.5 to 5 mM. When ATP (1.0 mM) and NaHCO_3 (1.0 mM) were held constant, various concentrations of AIR were tested ranging from 10 to 35 μ M. Finally, NaHCO_3 (1.0 mM) and AIR (10 μ M) were held constant when ATP concentrations were varied from 10 to 250 μ M. Initial velocity due to enzyme activity was determined for each experiment and Lineweaver-Burke plots of initial velocity versus varied bicarbonate, ATP or AIR concentration were generated to determine the likely mode of enzyme inhibition by 7-bromoisatin. Every data point on the Lineweaver-Burke plot was generated in duplicate and the mean of two experiments was used in Graphpad software package K_i calculations. Curve fittings were performed using the same software. Inhibition constants (K_i) and their standard errors with 95% confidence intervals for 7-bromoisatin with respect to AIR, ATP, and bicarbonate were determined using GraphPad Prism. The data for AIR were fitted by the program to equations 1-3 for uncompetitive enzyme inhibition while the data for ATP and bicarbonate was fitted into equation 4 based on the observed mixed kinetics. Inhibition constants for each inhibitor concentration were calculated separately and then averaged.

$$\frac{1}{V_0} = \frac{\alpha K_m}{V_{\max}} \times \frac{1}{[S]} + \frac{1}{V_{\max}} \quad (1),$$

$$\alpha = 1 + \frac{I}{K_i} \quad (2),$$

$$\alpha = \frac{\text{Slope}_{\text{inhibitor}}}{\text{Slope}_{\text{no inhibitor}}} \quad (3),$$

$$K_I = \frac{V_{\max}^{\text{app}}[I]}{\alpha (V_{\max} - V_{\max}^{\text{app}})} \quad (4),$$

where K_m is the Michaelis-Menten constant, αK_m is the apparent K_m in the presence of inhibitor, V_{max} is the maximum velocity, V_0 is the initial velocity, V_{max}^{app} is the apparent maximum velocity, $[S]$ is the substrate concentration, K_i is the binding constant, and the slopes with or without inhibitor are generated from a Lineweaver-Burk plot (61).

2.4.3 Synthesis of 5-aminoimidazole ribonucleotide (AIR)

AIR was prepared as described by Firestine *et al.* (62) with several modifications to the procedure. After purifying CAIR by a DEAE Sepharose column, fractions were analyzed by HPLC and UV spectroscopy for purity. CAIR fractions from the Sepharose purification were injected into HPLC and eluted isocratically with 50 mM DIPEAA at a flow rate of 1 mL/min. HPLC spectra were compared to the CAIR standard for the presence of impurities. In addition to HPLC, UV spectroscopy was used to analyze CAIR samples for identity and purity. Lyophilized CAIR fractions were dissolved in 100 mM Tris (pH 8.0), transferred to a 1-mL quartz cuvettes and each sample was scanned from 220 to 300 nm. UV spectra were compared to the published results for pure CAIR. (28) AIR was prepared by non-enzymatic decarboxylation of CAIR using NH_4OAc pH 4.8 buffer essentially as described by Firestine *et al.* Sepharose column purification was not necessary because pure CAIR was used for the decarboxylation reaction. This was validated by HPLC and UV analysis of the AIR produced (same conditions as for CAIR). The concentration of AIR used in the assays was determined using extinction coefficient (ϵ) of AIR at 260 nm ($\epsilon_{AIR} = 1570 \pm 100 \text{ M}^{-1}\text{cm}^{-1}$ at pH 8.0).

2.4.4 Preparation of diisopropylethylammonium acetate (DIPEAA)

Ninhydrin (large excess) was combined with N,N-diisopropylethylamine (DIPEA, 20 mL, 0.115 mol, 1.0 eq) and the reaction was stirred overnight at room temperature. Then, DIPEA solution was pipetted out to a new round-bottom flask followed by the addition of another large excess of ninhydrin. This mixture was refluxed overnight. After

24 hours, refluxing was stopped and the dark brown DIPEA solution was distilled to afford pure DIPEA. N,N-Diisopropylethylammonium acetate (DIPEAA) was produced by combining DIPEA with glacial acetic acid in a 1:1 ratio DIPEAA was diluted with HPLC grade water before use in HPLC.

CHAPTER 3

SMALL MOLECULES TARGETING BACTERIAL N^5 -CAIR MUTASE

3.1 Introduction

De novo purine biosynthesis is a key metabolic process found in higher eukaryotes, bacteria, yeasts, and plants (20). In recent years a dichotomy in the pathway has been found between species (Figure 3.1.1) (18). This divergence is centered on the formation and utilization of the chemically labile intermediate, N^5 -CAIR (63). Formation of N^5 -CAIR is accomplished by the enzyme N^5 -CAIR synthetase, which converts ATP, AIR and bicarbonate into N^5 -CAIR, ADP and inorganic phosphate. N^5 -CAIR mutase (class I PurE) directly transfers the carbamate carboxylate from the N^5 -position of N^5 -CAIR to C4 to generate CAIR. Animals, on the other hand, directly carboxylate AIR to produce CAIR using AIR carboxylase (class II PurE) (64, 65). It has been suggested that this difference in the pathways might be attributed to changes in the CO_2 environmental conditions (21).

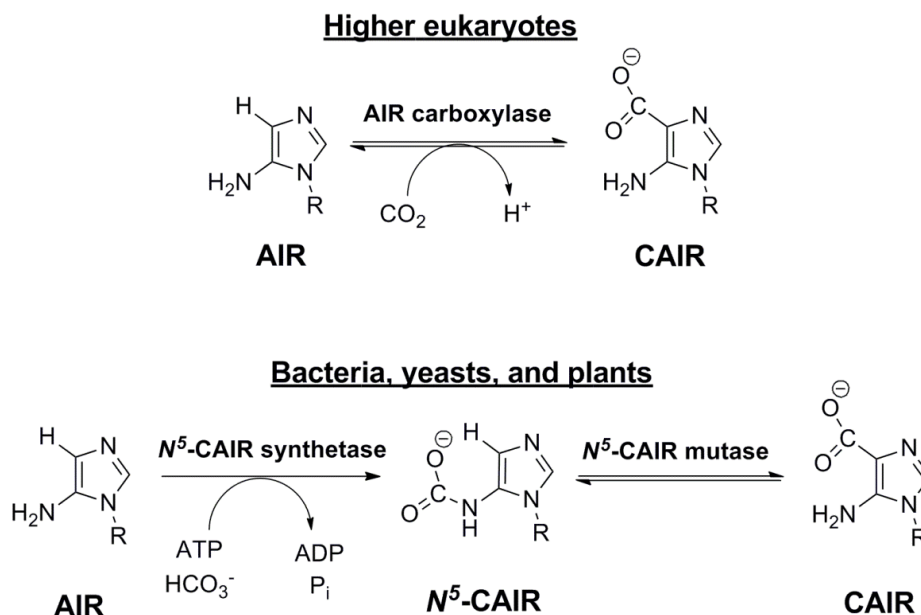


Figure 3.1.1 Reactions catalyzed by AIR carboxylase, N^5 -CAIR synthetase, and N^5 -CAIR mutase. R is ribose 5'-phosphate (66).

Structural and sequence alignment studies of AIR carboxylase and N^5 -CAIR mutase confirm that these enzymes are evolutionary related and they have a high degree of structural and sequence homology (Figure 3.1.2) (20, 67). Despite this similarity, biochemical studies of AIR carboxylase and N^5 -CAIR mutase show that the enzymes are highly specific for their own substrates. Thus, AIR carboxylase cannot utilize N^5 -CAIR as a substrate and N^5 -CAIR mutase is unable to catalyze a reaction of AIR and CO_2 (17). These shared features complicate the discovery of selective N^5 -CAIR mutase inhibitors.

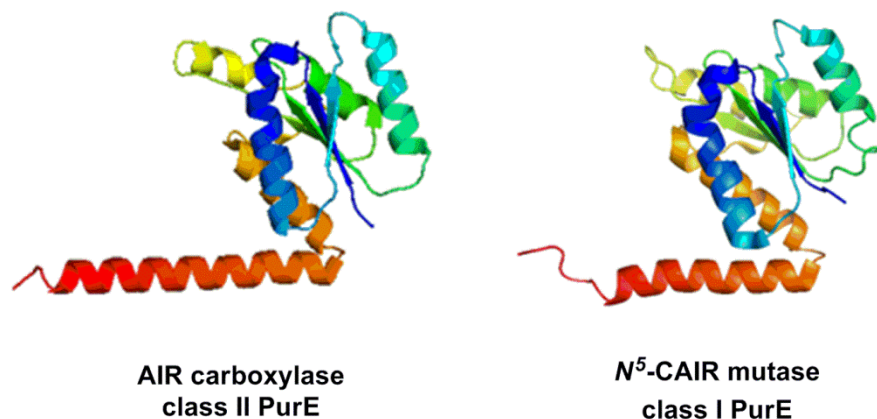


Figure 3.1.2 Comparison of two monomers: human AIR carboxylase (PDB 2H31) and *E. coli* N^5 -CAIR mutase (PDB 1D7A).

To date, there is only one example of a selective inhibitor between AIR carboxylase and N^5 -CAIR mutase. In 1993, Firestine *et al.* reported the discovery of NAIR (4-nitro-5-aminoimidazole ribonucleotide) (68). NAIR was shown to be a slow, tight-binding inhibitor of *G. gallus* AIR carboxylase with the inhibition constant (K_i) of 0.34 nM. Unfortunately, this compound inhibited AIR carboxylase better than N^5 -CAIR mutase, rendering the compound ineffective for antimicrobial studies. Furthermore, the compound did not possess drug-like properties because it was highly charged at

physiological pH. In a 2009 paper, Firestine and co-workers investigated multiple azole nucleotide analogs of NAIR as AIR carboxylase and N^5 -CAIR mutase inhibitors (67). However, these compounds were significantly less potent than NAIR, but still bound better to AIR carboxylase than N^5 -CAIR mutase. It was suggested that AIR carboxylase was sensitive to the electronic character of the nucleotide inhibitors and suggested that compounds which mimicked the electrostatic character of the transition state for the decarboxylation of N^5 -CAIR could become potent and selective N^5 -CAIR mutase inhibitors. However, no such inhibitors have been discovered.

Given the challenges listed above, coupled with the fact that no selective inhibitor of N^5 -CAIR mutase is known, it is clear that a new approach is needed to identify selective N^5 -CAIR mutase inhibitors. Therefore, we decided to take advantage of high-throughput technology and perform an unbiased search for potent and, more importantly, selective inhibitors of N^5 -CAIR mutase. In this chapter, the results of these studies will be outlined and the discovery of the first selective inhibitor of N^5 -CAIR mutase will be highlighted. The role that each stereoisomer plays in the potency and specificity of this molecule will be computationally explored and the initial efforts at developing a stereospecific synthesis of this inhibitor will be outlined.

3.2 Results

3.2.1 High-throughput Screening

In an attempt to identify drug-like compounds against N^5 -CAIR mutase, our laboratory initiated an HTS study at the Center for Chemical Genomics (CCG) at the University of Michigan. A 48,000 compound library of commercially available drug-like molecules was screened against *E. coli* N^5 -CAIR mutase with a counterscreen against human AIR carboxylase. The enzyme-catalyzed CAIR decarboxylation assay (Figure 3.2.1) was used for the HTS study. This assay was conducted by measuring the background UV absorbance (260 nm) in each well of the 384-well plate containing buffer, CAIR and the potential inhibitor from the 48,000-compound library. Then, the enzyme (*E. coli* N^5 -CAIR mutase or human AIR carboxylase) was added to each well and the absorbance was measured again after 10 minutes. The two absorbance measurements were subtracted to give the absorbance due to enzyme activity without background. It was important to measure the background levels because it was likely that some library compounds absorbed UV light at 260 nm.

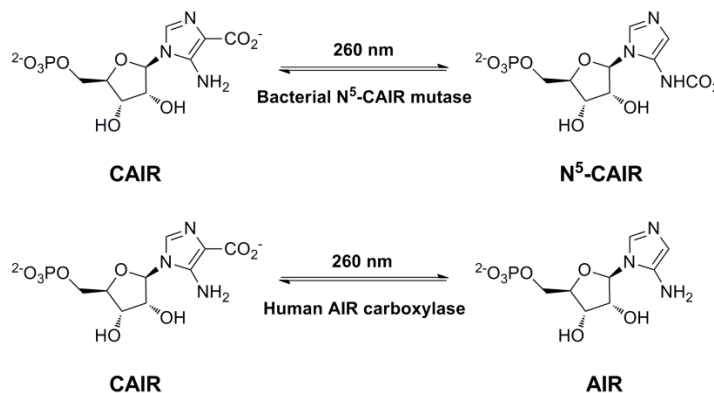


Figure 3.2.1 Enzyme-catalyzed CAIR decarboxylation assay.

The high-throughput screen was conducted as follows. First, 48,000 compounds were screened against *E. coli* N^5 -CAIR mutase at a single inhibitor concentration. The

activity of the inhibitor was determined relative to the positive control (no enzyme) and a negative control (no inhibitor). The primary screen identified 1,637 compounds with a hit rate of 3.4% (Figure 3.2.2). The second screen (in triplicate) validated 360 out of the 1,637 compounds yielding a hit rate of 0.75%. Out of 360 compounds, 259 followed Lipinski's rules (44).

Dose-response studies were conducted on all 259 compounds and 130 displayed a dose-response relationship (hit rate of 0.27%). Finally, dose-response studies were conducted on all 130 compounds against human AIR carboxylase to establish their selectivity profiles. Only two compounds (hit rate 0.004%) out of 130 did not inhibit human AIR carboxylase at the concentrations screened by CCG.

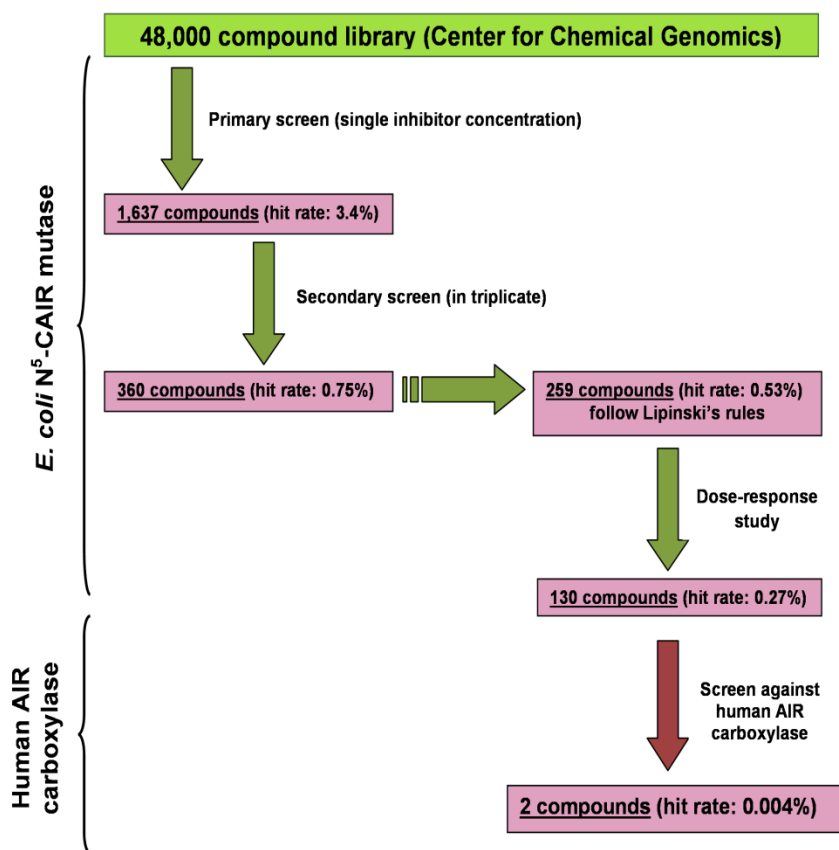
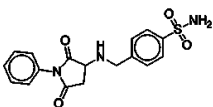
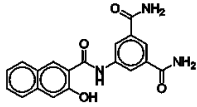
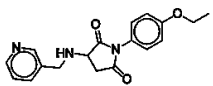
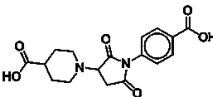
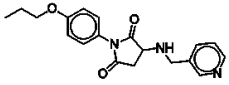
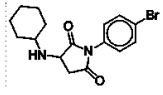


Figure 3.2.2 HTS flow chart.

Examination of the 130 *E. coli* N^5 -CAIR mutase inhibitors revealed several desired features (Table 3.2.1). The two selective inhibitors (**1**, **2**) of *E. coli* N^5 -CAIR mutase are also shown in Table 3.2.1. Compound **1** displayed an IC_{50} of 20 μ M against bacterial enzyme while it showed no activity against human enzyme below 100 μ M (the highest concentration screened). Compound **2** showed similar potency with IC_{50} against *E. coli* N^5 -CAIR mutase of 12 μ M and again it was not active against human AIR carboxylase. The remaining compounds displayed low micromolar IC_{50} values against both N^5 -CAIR mutase and AIR carboxylase and thus were not selective. Interestingly, the majority of the 130 compounds were similar to compound **1**. As can be seen from the representative examples shown in Table 3.2.1, these compounds had different substituted amines; however, these substitutions did not result in selectivity. Only the sulfonamide of **1** gave selective activity, albeit at a loss of inhibitor potency.

Table 3.2.1 HTS-derived inhibitors of *E. coli* N^5 -CAIR mutase and human AIR carboxylase

No.	Structure	IC_{50} N^5 -CAIR Mutase (μ M)	IC_{50} AIR Carboxylase (μ M)	No.	Structure	IC_{50} N^5 -CAIR Mutase (μ M)	IC_{50} AIR Carboxylase (μ M)
1						12	>100
3						3	2
5						27	50

3.2.2 Kinetic Analysis of “Hit” Compounds

Compounds **1** and **2** were acquired from the vendor to perform verification of the HTS results. Kinetic analysis of both inhibitors was conducted using the same enzyme-catalyzed decarboxylation assay as previously described in the introduction (Figure 3.2.1). Lineweaver-Burk plots were constructed to determine the inhibition constants (K_i) and the mode of inhibition (competitive, uncompetitive, or non-competitive) of compounds **1** and **2** against *E. coli* N^5 -CAIR mutase and human AIR carboxylase. The results are presented in Figure 3.2.3. Compound **1** was competitive with respect to CAIR when tested against both N^5 -CAIR mutase and AIR carboxylase. The inhibition constant, K_i was $28 \pm 5 \mu\text{M}$ against the bacterial enzyme and $134 \pm 21 \mu\text{M}$ against the AIR carboxylase. Although, **1** displayed only a 5-fold lower K_i for N^5 -CAIR mutase than for AIR carboxylase, it is the first known, selective inhibitor of the bacterial enzyme.

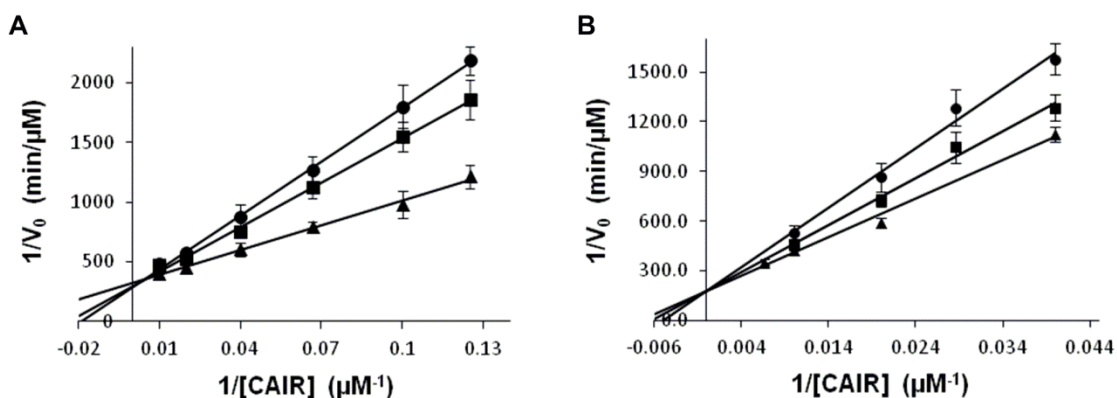


Figure 3.2.3 (A) Lineweaver-Burke plot for the inhibition of *E. coli* N^5 -CAIR mutase in the presence of (▲) no inhibitor, (■) $25 \mu\text{M}$ of **1**, and (●) $35 \mu\text{M}$ of **1**. (B) Lineweaver-Burke plot for the inhibition of human AIR carboxylase in the presence of (▲) no inhibitor, (■) $35 \mu\text{M}$ of **1**, and (●) $75 \mu\text{M}$ of **1**.

Generation of a Lineweaver-Burke plot for compound **2** failed because this compound strongly absorbed UV light at 260 nm creating large errors in the measurement of enzyme-catalyzed decarboxylation. In addition, **2** was unique and structurally unrelated to any other “hit” from the HTS. Based on the above data, it was concluded that compound **2** was probably a false HTS positive.

3.2.3 Molecular Modeling Study of Compound **1**

To gain insight into the selectivity of **1** for N^5 -CAIR mutase versus AIR carboxylase, we conducted molecular modeling studies based on the available crystal structures of the bacterial and human enzymes. Our kinetic analysis of compound **1** (Figure 3.2.3) showed that it was a competitive inhibitor (with respect to CAIR) of N^5 -CAIR mutase and AIR carboxylase. This indicated that compound **1** bound to the same active-site pocket as CAIR. Based on this information, docking of **1** was carried out using the MOE (2010.10) software package with the crystal structure of *E. coli* N^5 -CAIR mutase (PDB: 2ATE), which had the CAIR analog, NAIR (Figure 3.2.4), bound in the active site. Unfortunately, human AIR carboxylase (PDB: 2H31) had no substrates or products bound in its active site. Since N^5 -CAIR mutase and AIR carboxylase were previously found to be evolutionary related and displayed nearly identical tertiary structures with a high degree of sequence similarity (39, 69), we superimposed the two enzymes to determine the location of the CAIR binding site in AIR carboxylase.

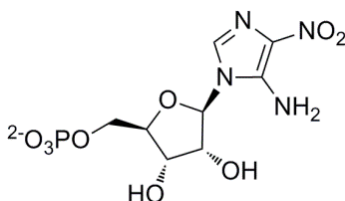


Figure 3.2.4 Structure of NAIR.

The examination of compound **1** revealed that there was one chiral center and the kinetic analysis of **1** (Section 3.2.2) was performed using the commercially acquired racemic mixture. Unfortunately, pure enantiomers of compound **1** were not commercially available and thus, we were unable to determine the effect of stereochemistry on the potency of inhibition. To examine a possible effect, both enantiomers of inhibitor **1** (Figure 3.2.5) were included in the docking studies to gain additional information about the selectivity of one enantiomer versus another.

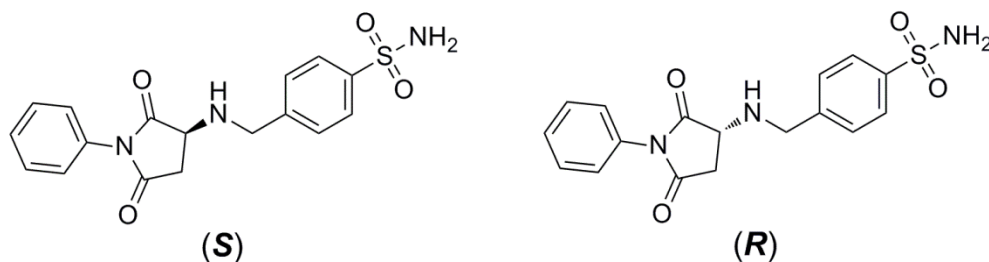


Figure 3.2.5 Structures of (*S*) and (*R*) enantiomers of compound **1**.

Docking studies revealed that neither enantiomer of **1** bound deeply into the active site of AIR carboxylase (Figures 3.2.6, 3.2.7 and 3.2.8, 3.2.9) and thus was more solvent exposed. Compound **1** formed strong hydrogen bond interactions with Arg331 as well as Lys304, both of which are conserved in all AIR carboxylases. These interactions were formed with the succinamide and sulfonamide moieties of **1** and served to anchor the compound in a solvent exposed region of the active site pocket. In contrast, **1** bound better to *N*⁵-CAIR mutase (Figures 3.2.10, 3.2.11 and 3.2.12, 3.2.13) possibly due to the stronger enzyme interactions with residues Ala96, Ala73, and Arg46, which were conserved only in *N*⁵-CAIR mutases. These enzyme residues also had strong hydrogen bond interactions with a sulfonamide moiety of **1** along with two π -cation interactions. Due to their location on the enzyme, Ala96, Ala73 and Arg46 caused **1** to bind deeper

into the pocket resulting in an increased number of interactions with other residues in the active site of N^5 -CAIR mutase.

Additionally, the evaluation of both enantiomers (R versus S) was performed separately within each enzyme class. Docking studies showed that the enantiomers had differences in their binding affinity (as measured by binding energies) for each enzyme. This suggested that an increase in selectivity may be gained by focusing on only one enantiomer of compound **1**. It was found that the (S)-isomer of **1** had a lower energy values than the (R)-isomer in both N^5 -CAIR mutase (-15.06 kcal/mol for (S) and -13.94 kcal/mol for (R)) and AIR carboxylase (-12.66 kcal/mol for (S) and -9.12 kcal/mol for (R)).

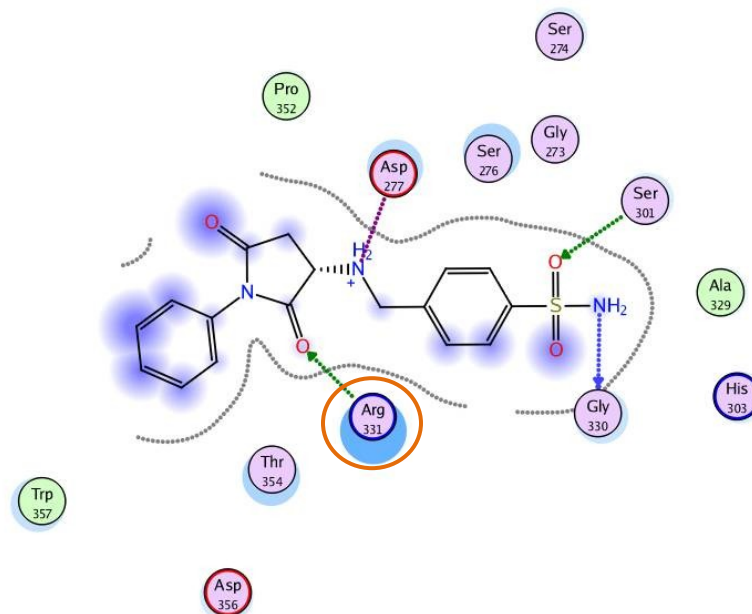


Figure 3.2.6 Interaction diagram of (S) isomer of compound **1** docked to human AIR carboxylase active site (PDB: 2H31). The red circle around a residue indicates that this residue is strictly conserved in human AIR carboxylase. The intensity of the purple color around an atom in the compound indicates the degree of solvent exposure. Dotted arrows represent hydrogen bond interactions between ligand and the enzyme. Hydrophobic residues are colored in green interior while polar residues are colored in

light purple. Basic and acid residues are annotated with a blue or red ring, respectively, around a residue. The size of the light blue crescent around a residue indicates the strength of the interaction. Only residues within 5 Å from compound **1** are shown.

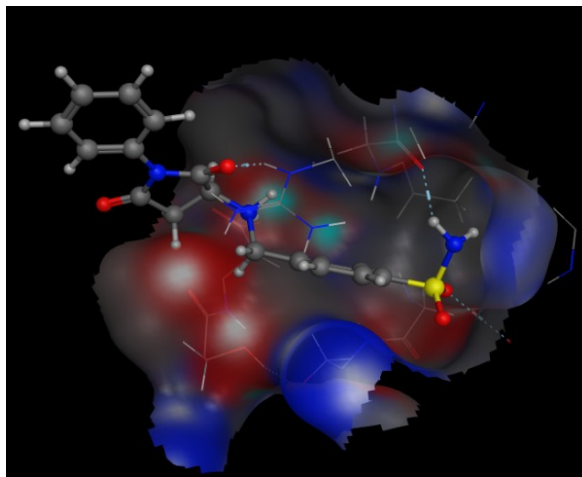


Figure 3.2.7 The surface representation of human AIR carboxylase active site with (*S*) enantiomer of **1**. All residues shown on the 3D diagram are located within 5 Å from molecule **1**. Blue color represents basic residues and red color shows acidic residues.

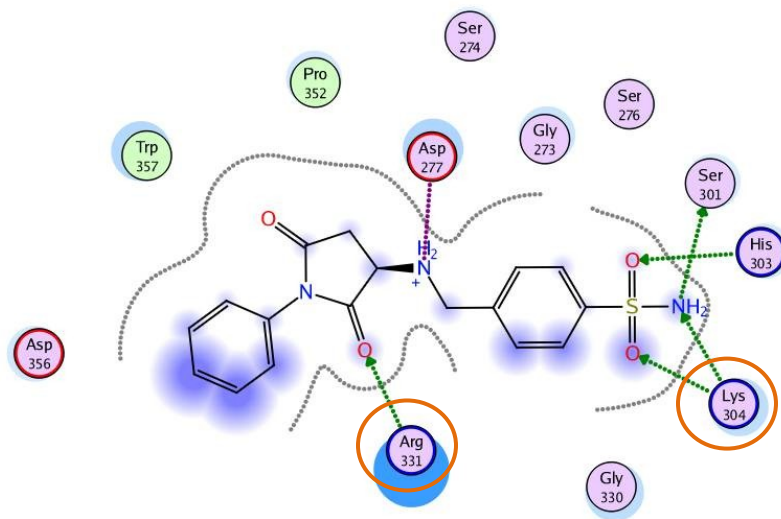


Figure 3.2.8 Interaction diagram of (*R*) isomer of compound **1** docked to human AIR carboxylase active site (PDB: 2H31). The nomenclature of the diagram is the same as described for Figure 3.2.6.

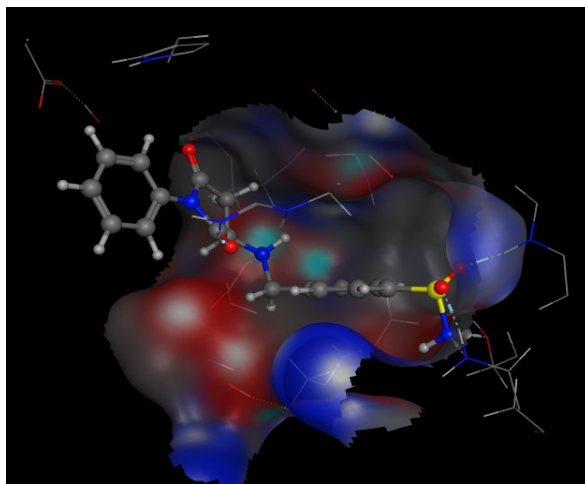


Figure 3.2.9 The surface representation of human AIR carboxylase active site with (*R*) enantiomer of **1**. The nomenclature of the diagram is the same as described for Figure 3.2.7.

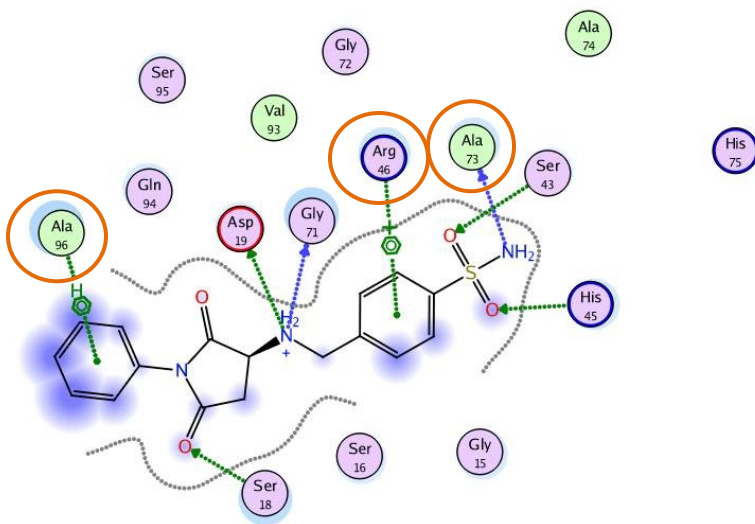


Figure 3.2.10 Interaction diagram of the (*S*)-isomer of compound **1** docked to *E. coli* N^5 -CAIR mutase active site (PDB: 2ATE). The red circle around a residue indicates that this residue is strictly conserved in *E. coli* N^5 -CAIR mutase. The rest of the nomenclature is the same as described for Figure 3.2.6.

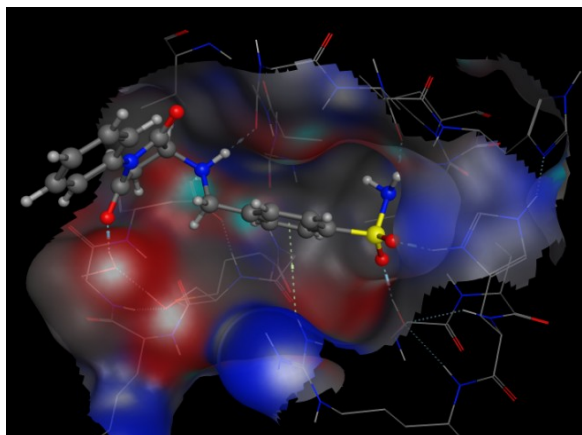


Figure 3.2.11 The surface representation of *E. coli* N^5 -CAIR mutase active site with (*S*) enantiomer of **1**. The nomenclature of the diagram is the same as described for Figure 3.2.7.

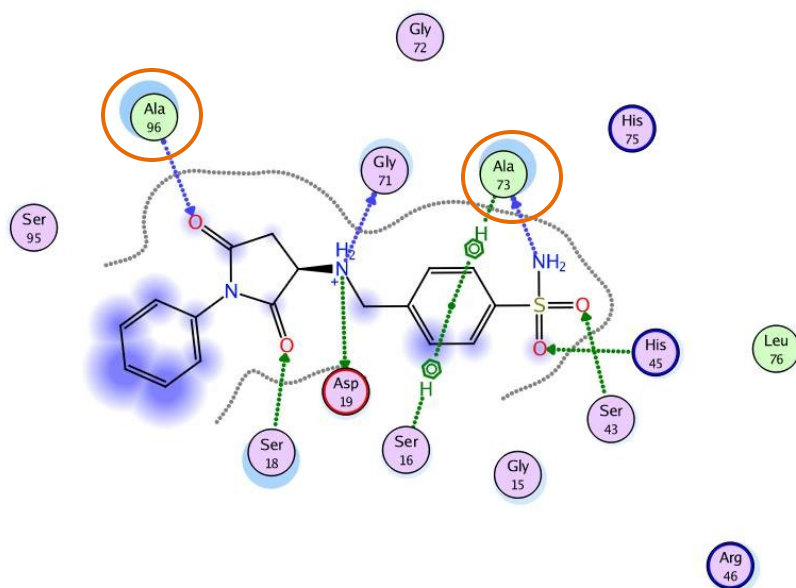


Figure 3.2.12 Interaction diagram of (*R*) isomer of compound **1** docked to *E. coli* N^5 -CAIR mutase active site (PDB: 2ATE). The nomenclature of the diagram is the same as described for Figure 3.2.10.

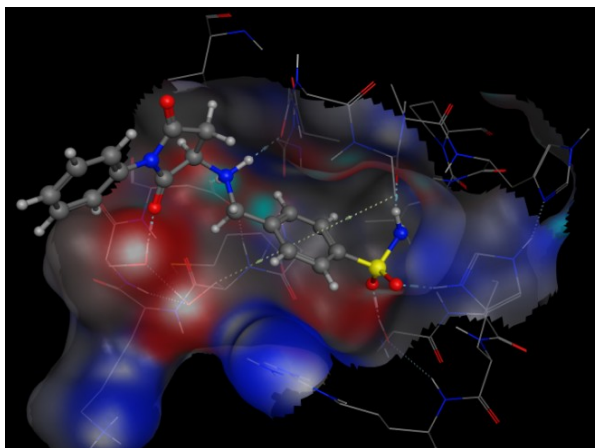


Figure 3.2.13 The surface representation of *E. coli* N^5 -CAIR mutase active site with (*R*) enantiomer of **1**. The nomenclature of the diagram is the same as described for Figure 3.2.7.

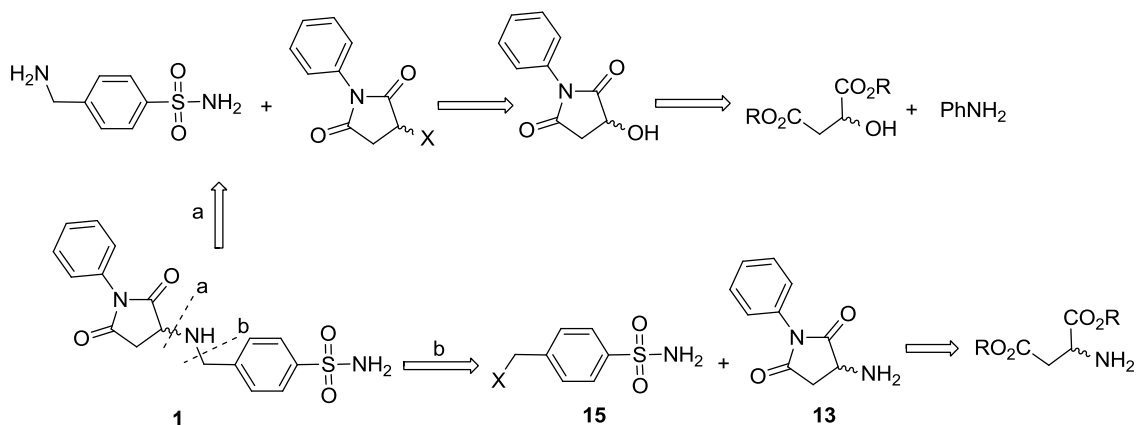
3.2.4 Exploratory Synthesis of the Pure Enantiomers of Compound **1**

The molecular modeling studies (Section 3.2.3) suggested the possibility that the (*S*)-isomer of compound **1** was a better inhibitor than the (*R*)-isomer. To test this molecular modeling hypothesis, the enantiomerically pure isomers of **1** were required for the evaluation against each enzyme. Unfortunately, the synthetic method for the preparation of these isomers was unknown and there were no publications on **1** reported in any database. Thus, preliminary studies were required to explore the stereospecific synthesis of **1**.

A retrosynthetic analysis was conducted for the synthesis of **1**. Compound **1** could be divided at points **a** or **b**. Dissection at **a** gave two products, 4-aminomethyl benzenesulfonamide and the stereospecific halide. It was hypothesized that this halide could be synthesized from the corresponding alcohol which was produced by the condensation of the stereospecific 2-hydroxy-butanoic acid ethyl ester with aniline. A disconnection at **b** would give the stereospecific amine and the corresponding

sulfonamide halide. The amine could be synthesized from a protected aspartic acid and aniline. Analysis of route **a** revealed that while the aminomethyl-benzenesulfonamide was commercially available, there were no reported stereospecific syntheses of the halide. However, cyclization of the butanoic acid had been reported in the literature. For route **b**, both the stereospecific amine and the benzenesulfonamide methyl halide had been previously reported in the literature. Although there were several concerns regarding the control of the addition of the halide to the amine, the short synthesis coupled with the fact that all of the compounds were known, indicated that route **b** would likely be the preferred method for preparation of the pure enantiomers of compound **1**.

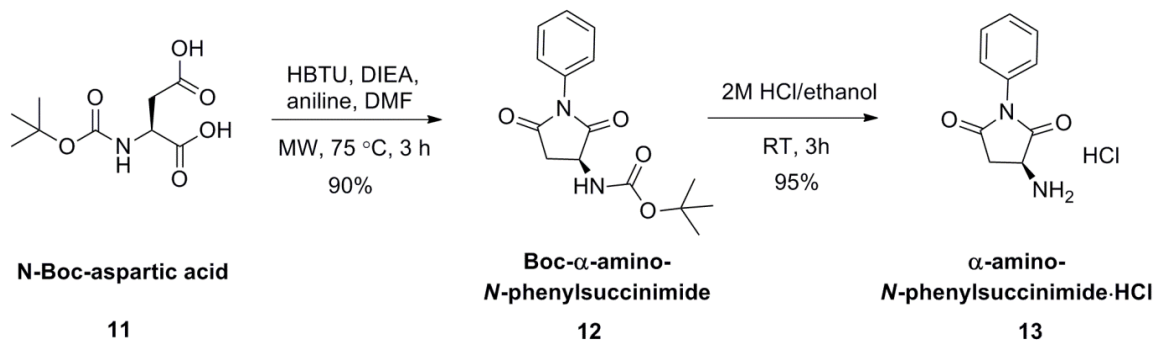
Scheme 3.1 Retrosynthetic analysis for the synthesis of compound **1**.



The synthesis of compound **1** began with the preparation of the amine **13** in two steps (Scheme 3.2). The first step consisted of a microwave-assisted cyclization reaction of *N*-Boc-*S*-aspartic acid with aniline in the presence of *O*-(Benzotriazol-1-yl)-*N,N,N',N'*-tetramethyluronium hexafluorophosphate (HBTU) and *N,N*-diisopropylethylamine (DIEA) in DMF to afford compound **12** in 90% yield. This one-step microwave-assisted coupling reaction was fast and high yielding compared to the published procedure (70) by Witiak *et al.* that reported preparation of compound **12** in 3 steps. Synthesis of **13** from **12** was

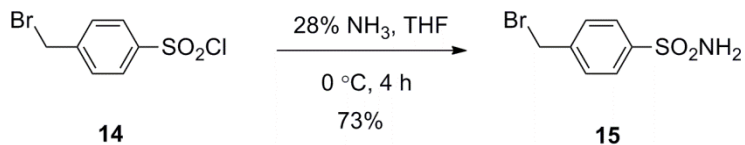
accomplished by standard *tert*-butyloxycarbonyl (Boc) group deprotection using 2M hydrochloric acid in ethanol to afford the desired compound in high yields.

Scheme 3.2 Synthesis of Boc- α -amino-*N*-phenylsuccinimide **12** and α -amino-*N*-phenylsuccinimide·HCl **13**.



The availability of stereochemically defined compound **13** allowed examining multiple routes toward the preparation of the enantiomers of **1**. A review of the literature suggested several synthetic approaches to secondary amines from primary amines including direct *N*-alkylation (71-73), the use of protective groups (74, 75), and reductive alkylation reaction (76, 77). First, it was decided to proceed with the direct *N*-alkylation of compound **13** with **15**. Compound **15** was prepared from the commercially available **14** by treatment with 28% ammonia in tetrahydrofuran (THF) (Scheme 3.3) (78).

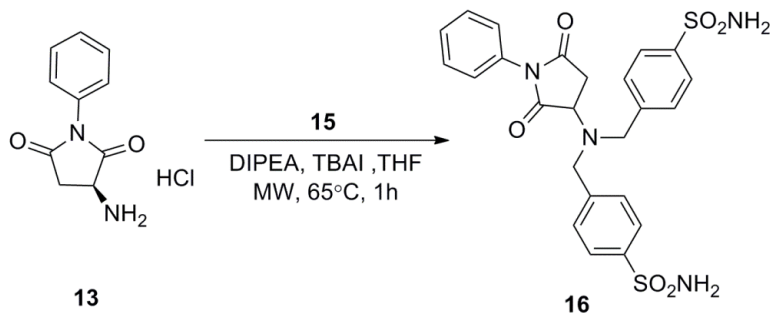
Scheme 3.3 Synthesis of compound **15**.



Reaction of **13** with **15** in the presence of triethylamine at 0°C resulted in no reaction. Repeating this reaction using a different base, diisopropylethylamine (DIPEA) with tetrabutylammonium iodide (TBAI) in THF while heating in the microwave produced

exclusively the di-alkylated compound **16** (Scheme 3.4). Examination of direct *N*-alkylation of compound **13** with compound **15** in the presence of cesium hydroxide monohydrate in dimethylsulfoxide (DMF) was also unsuccessful and yielded no reaction.

Scheme 3.4 Direct *N*-alkylation reaction of **13** with **15**.

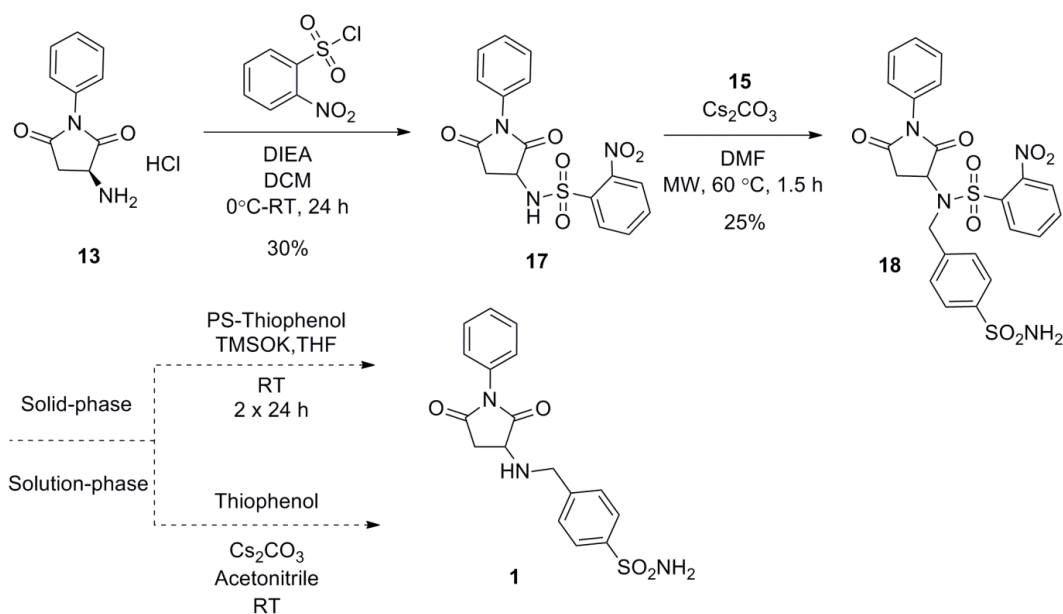


Since the direct alkylation of **13** resulted in only the dialkyl product **16**, the exploration of the option of protecting the amine to prevent di-addition was attempted. Previous researchers have utilized the nosyl (4-nitrobenzenesulfonyl) protecting group as a mechanism for controlling alkylation reactions of amines (79). This protecting group converts an amine into a sulfonamide which increases the acidity of the NH proton allowing for more facile alkylation, but also prevents the over-alkylation of the amine. Furthermore, the nosyl group can be readily removed.

Protection of **13** with 4-nitrobenzenesulfonyl chloride (Nosyl-Cl) in dichloromethane (DCM) afforded compound **17** in 30% yield (Scheme 3.5). Next, the alkylation of **17** was examined. After the exploration of numerous methods, it was found that the microwave-assisted alkylation of **17** in the presence of cesium carbonate produced the desired compound **18** albeit in low yields. The final step was the removal of the protecting group. Nosyl protecting groups were removed by treatment with thiols where thiophenol was the most common reagent (80). Deprotection of **18** with thiophenol and cesium carbonate in acetonitrile resulted in either no reaction or highly

decomposed materials depending upon the conditions utilized in the reaction. We also explored a solid-phase route by reacting **18** with polystyrene-thiophenol in the presence of potassium trimethylsilanolate (TMSOK) in THF (**81**). Again, only highly decomposed materials were obtained.

Scheme 3.5 Synthetic approach for the synthesis of compound **1** using 4-nitrobenzenesulfonyl chloride as protective agent.



3.3 Discussion

Researchers working in the area of the *de novo* purine biosynthesis consider Buchanan and co-workers, working in the 1950's, as pioneers in establishing the basics of this fundamental pathway. In the 1990s, it was realized that major differences in the *de novo* purine biosynthesis existed between humans and microbes (28, 29, 82). These findings suggested that exploring the divergence in this pathway could result in the development of novel antimicrobial agents (17, 64, 65). Despite the predictions, medicinal agents targeting bacterial N^5 -CAIR mutase and synthetase have been limited.

One of the most difficult challenges in this field is the development of agents that specifically target bacterial N^5 -CAIR mutase. Both structural and sequence studies have revealed that N^5 -CAIR mutase is highly similar to human AIR carboxylase. To date, there have been no selective inhibitors reported and most of the known inhibitors of these enzymes possess more potent inhibition against AIR carboxylase over N^5 -CAIR mutase. To accomplish the main goal of discovering selective N^5 -CAIR mutase inhibitors, the University of Michigan high-throughput facility has been successfully utilized. The discovery of a moderately potent and selective *E. coli* N^5 -CAIR mutase inhibitor **1** ($K_i = 28.4 \pm 5 \mu\text{M}$) represents a groundbreaking step towards the main goal of developing novel antibiotics targeting the *de novo* purine biosynthetic pathway.

The selectivity of compound **1** was a key question that has arisen from this discovery. Previous studies of inhibitors of AIR carboxylase and N^5 -CAIR mutase have postulated that stereoelectronics have played a key role in selectivity (67). Given the fact that approximately 100 additional molecules related to **1** have been discovered, this suggests that unlike the previous studies, the substitution patterns on **1** are critical for its selectivity. To gain an understanding of how the substitutions on **1** affect the selectivity,

docking studies to probe molecular interactions between **1** and both enzymes have been conducted.

It was found that **1** had alternative binding interactions with active site residues of *N*⁵-CAIR mutase compared to AIR carboxylase. Mathews *et al.* have previously showed that residues in the P-loop and 40s loop were conserved between AIR carboxylase and *N*⁵-CAIR mutase while residues within the 70s loop were conserved strictly within the enzyme class (18). Therefore, it was expected that residues within the 70s loop would form distinct interactions which in turn would explain the differences in the binding specificity of **1**. Molecular modeling revealed that Ala73 (*N*⁵-CAIR mutase) and Arg331 (AIR carboxylase), both part of the 70s loop, did form a strong hydrogen bond interactions to the succinamide and sulfonamide moieties of **1**. Moreover, the conserved Arg46 in *N*⁵-CAIR mutase and Lys304 in AIR carboxylase were also involved in binding of **1**. Even though, Arg46 and Lys304 belonged to the conserved 40s loop, previous research indicated that these residues were a distinctive feature within each enzyme class (83). Earlier reports had not postulated any importance for the residues located in the 90s loop, but Ala96, present only in *E. coli* *N*⁵-CAIR mutase provided key interactions to **1**. Other residues involved in the binding of **1** included Ser16, Ser18, Asp19, Ser43, His45, Gly71 on *E. coli* *N*⁵-CAIR mutase and Asp277, Ser301, His303, and Gly330 on human AIR carboxylase. All of these amino acids were conserved within each enzyme class and likely explain why so many compounds related to **1** were capable of binding to both enzymes. Since *E. coli* *N*⁵-CAIR mutase had more residues interacting with **1** than human AIR carboxylase and the strength of those interactions was much higher (~2-4 kcal/mol), it was concluded that **1** was selective for *N*⁵-CAIR mutase.

Another feature that was examined during the docking study was the role that stereochemistry played in binding. The molecular modeling of compound **1** enantiomers

showed strong evidence that the (*S*)-isomer had higher binding energy (~1-3 kcal/mol) for *N*⁵-CAIR mutase and AIR carboxylase than its (*R*)-isomer. These results prompted us to begin examining whether the (*S*) isomer might lead to a more effective inhibitor of the bacterial *N*⁵-CAIR mutase. Therefore, the study into the stereospecific synthesis of **1** was initiated. Unfortunately, no synthetic method for preparation of **1** was found in the literature. Our approach towards the enantiomeric synthesis of **1** focused on the alkylation of **13**, prepared from aspartic acid derivatives. Generally, secondary amines can be made by N-alkylation of primary amines under conditions which minimize di-addition. In our case, steric and stereochemical considerations prevented the synthesis of the (*S*)-isomer of **1**. Several modifications to the alkylation procedure where no heat was applied gave no reaction, while heating lead to the rapid formation of the di-alkylated product. While we could have employed a strong base to generate the amino anion, this would have likely led to racemization. Thus, the protection of amine with nosyl chloride was attempted to afford compound **17**. Protection was found to be very low yielding (30%) most likely due to the bulkiness of the starting materials which prevented proper molecule orientation for the nucleophilic attack. Given this conjecture that steric bulk was responsible for the difficulty in formation of **17**, it was perhaps not surprising that formation of the mono-alkyled product **18** was also accomplished in poor yield. Despite the low yield, it was hypothesized that the final product could be achieved by deprotection. However, cleavage of the nosyl protecting group by two different routes gave only decomposition of the starting materials.

While we were ultimately unsuccessful in the stereospecific synthesis of **1**, the optimization of the synthesis of the key intermediate **13** was successful and several methods for the alkylation of this amine were also explored. In addition, polarimetry experiments (Table 3.4.1, page 58) showed that the synthesis of the pure enantiomer of

compound **13** was achieved without any product racemization. There are other methods which could be employed to prepare **1**, including reductive alkylation or even abandoning route **b** and exploring route **a** outlined in scheme 3.1. This will likely be the subject of future work in the Firestine laboratory.

3.4 Materials and Methods

Analytical HPLC experiments were performed on a Waters 600 instrument using PRP1 reversed-phase column (Hamilton). Enzymatic assays were conducted on a Varian UV-vis Cary 100 spectrophotometer equipped with a cell changer and a temperature controller. Microwave irradiation experiments were carried out on a Biotage Initiator instrument operating at 2.45 GHz frequency with continuous irradiation power from 0 to 400 W. Synthesized compounds were purified using FlashMaster II Purification System. Measurements of pH were performed on Acumet AB15 pH meter (Fisher Scientific). The ^1H and ^{13}C NMR spectra were recorded with permission on a Varian 400 MHz at the Wayne State University Chemistry Department. Deuterated solvents were acquired from Cambridge Isotopes. Inhibitors **1** and **2** were purchased from Maybridge. All other chemicals were obtained from Fisher Scientific, Sigma-Aldrich, Acros Organics, TCI, Chem-Impex International or VWR International.

3.4.1 High-throughput screening

HTS screen was conducted at the Center for Chemical Genomics (CCG) at the University of Michigan. The 48,000 compound library was constructed using 16,000 compounds from the Maybridge Hit-Finder library (Maybridge), 20,000 compounds from ChemDiv, 10,000 compounds from Chembridge, and 2,000 compounds from the MS Spectrum library. The assay for both N^5 -CAIR mutase and AIR carboxylase involved monitoring the enzyme catalyzed decarboxylation of CAIR at 260 nm. *E. coli* N^5 -CAIR mutase, human AIR carboxylase, and CAIR were prepared as previously described (84). All assays were performed in 384-well plates (Corning 3701) as follows. To each assay well, buffer (100 mM Tris·HCl pH 8.0), 10 μM CAIR and a library member (10-20 μM depending upon supplier) were added and the absorbance of each well was measured at 260 nm. The reaction was initiated by the addition of *E. coli* N^5 -CAIR mutase and the

reaction was quenched by the addition of 10 mM NaOH after 10 minutes. The absorbance of each well was again measured and the two measurements were subtracted. For the positive control, no drug or enzyme was added while the negative control consisted of no drug but added enzyme. The positive control values were set to 100% inhibition while the negative control was set to 0%. Compounds which displayed a 3 standard deviation difference from the negative control were taken as potential inhibitors. All potential inhibitors were rescreened, in triplicate, using the same assay under the same conditions. Only compounds which displayed inhibition in all three replicates were analyzed further. Lastly, an 8-point dose-response assay was conducted with drug concentrations ranging from 1-100 μ M. The dose-response assay was conducted using N^5 -CAIR mutase or human AIR carboxylase.

3.4.2 Purification of Human AIR Carboxylase

Human AIR carboxylase was purified from overexpressed *E. coli* BL21-DE3 using a plasmid containing cloned Ade2 gene with a His-tag as prepared by Dr. Paritala. Purification of AIR carboxylase was conducted as follows (40). Bacterial cells expressing AIR carboxylase were lysed using the B-PER reagent (4 mL per gram of pellet, Pierce Biotechnologies). The lysed bacteria were centrifuged at 14,500 rpm for 60 min (Beckman ultra high-speed centrifuge, rotor JA-20). Streptomycin (5 mg/mL) was added to the supernatant, incubated for 30 min and then centrifuged at 14,500 rpm for 60 min. The supernatant was loaded onto a column containing Cobalt RAPID RUN™ Agarose Beads (Gold Biotechnology) which had previously been pre-conditioned with buffer A (50 mM sodium phosphate, 300 mM sodium chloride, and 10 mM imidazole, pH 7.4 at 4°C). The protein loaded column was successively washed, at 4 °C, with Buffers B-D (50 mM sodium phosphate, pH 7.4, 300 mM sodium chloride, containing either 25 mM (B), 50 mM (C), or 100 mM (D) imidazole.. AIR carboxylase was eluted with buffer E containing

50 mM sodium phosphate, 300 mM sodium chloride, and 150 mM imidazole, pH 7.4 at 4°C. The purity of the protein was checked with SDS-PAGE (47 kDa band). Purified AIR carboxylase was dialyzed against 10 mM Tris·HCl, 200 mM NaCl, pH 8 and concentrated to 1 mg/mL using an Amicon centrifugal concentrator.

3.4.3 Kinetic analysis of inhibitor 1

All assays were performed using a Cary 100 UV-vis spectrophotometer, thermostated to 37 °C and reagents were kept on ice until use. In a 1-mL cuvette, 100 mM Tris-HCl pH 8.0, varied amounts of CAIR (5-100 μM) and compound **1** or **2** (0 - 100 μM) were combined followed by a 2 min incubation time at 37 °C. Background UV absorbance was measured and the reaction was initiated by the addition of 260 ng of *E. coli* N5-CAIR mutase. The conversion of CAIR to *N*⁵-CAIR was monitored at 260 nm. The initial velocity was determined over a two minute time span immediately after addition of the enzyme. The assay for AIR carboxylase was carried out in an identical fashion as listed above except that the reaction was initiated by the addition of 560 ng of human AIR carboxylase enzyme. Lineweaver-Burke plots for both enzymes were constructed by plotting 1/*V*₀ vs. 1/[S] and linear lines were calculated using GraphPad Prism. Inhibition constant (*K*_i) and the standard error with 95% confidence interval were calculated using the GraphPad Prism software package. The data for compound **1** were fitted by the program to equations 1-3 for competitive enzyme inhibition.

$$\frac{1}{V_0} = \frac{\alpha K_m}{V_{max}} \times \frac{1}{[S]} + \frac{1}{V_{max}} \quad (1)$$

$$\alpha = 1 + \frac{I}{K_i} \quad (2)$$

$$\alpha = \frac{\text{Slope}_{\text{inhibitor}}}{\text{Slope}_{\text{no inhibitor}}} \quad (3)$$

In these equations, K_m is the Michaelis-Menten constant, αK_m is the apparent K_m in the presence of the inhibitor, V_{max} is the maximum velocity, V_0 is the initial velocity, $[S]$ is the substrate concentration, and K_i is the binding constant (85)

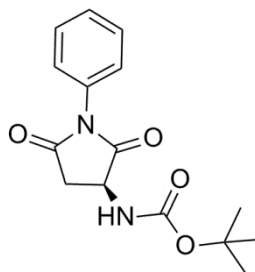
3.4.4 Molecular modeling studies

All molecular modeling studies were performed on a Pentium IV Windows XP workstation using the Molecular Operating Environment (MOE 2010.10; Chemical Computing Group, Canada) software package. The crystal structures of *E. coli* N^5 -CAIR mutase complexed with nitroAIR (PDB ID: 2ATE) and AIR carboxylase complexed with CO_2 (PDB ID: 2H31) were obtained from the protein data bank. N^5 -CAIR mutase was prepared for docking studies by removing nitroAIR and water molecules from the active site; applying Protonate3D function on the whole enzyme to correct for the physiological pH of 7.4; isolating the active site pocket and calculating partial charges on the active site residues using the MMFF94x force field. Human AIR carboxylase was a part of a bifunctional enzyme called phosphoribosylaminoimidazole carboxylase/phosphoribosylaminoimidazole succinocarboxamide synthetase (PAICS). Therefore, the AIR carboxylase components of PAICS were isolated from the rest of the enzyme and prepared in a manner identical to those described for N^5 -CAIR mutase. To determine the location of the active site of AIR carboxylase, *E. coli* N^5 -CAIR mutase was superimposed with human AIR carboxylase and the region of AIR carboxylase which overlapped with residues binding NAIR in N^5 -CAIR mutase was taken to be the active site of AIR carboxylase. Isomers of compound **1** were drawn using the builder module of MOE followed by the calculation of partial charges using the MMFF94x force field. Ligand-receptor docking of two isomers of compound **1** with either *E. coli* N^5 -CAIR mutase or human AIR carboxylase was carried out using MOE 2010.10 docking function. The poses were scored based on the London dG scoring function (Retain: 30) for estimating

binding energy. Refinement was set to Forcefield (Interactions: 500) in order to minimize energy in the receptor pocket. Finally, the Rescoring 2 option was set to none (Retain: 10), allowing the final refined poses to be ranked by the MM/GBVI binding energy estimation. Multiple, low energy conformations of each isomer were calculated and the results were stored in a database. Docking positions of each isomer in the active sites of *N*⁵-CAIR mutase and AIR carboxylase were significantly affected by their available conformations. Therefore, the lowest energy conformer of each isomer was chosen from the database for further analysis. Ligand binding energies were calculated for docked poses using the appropriate function available in MOE.

3.4.5 Exploratory synthesis of compound 1

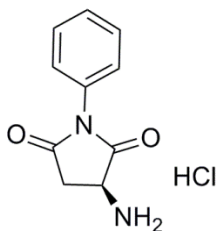
Boc- α -amino-*N*-phenylsuccinimide (12)



N-Boc-L(S)-aspartic acid (1.0 g, 4.29 mmol, 1 eq) and HBTU (1.6 g, 4.29 mmol, 1 eq) were dissolved in 15 mL of anhydrous DMF in a 20 mL microwave vial (Biotage). The reaction vessel was sealed, purged with argon gas, and stirred for 15 min until all solids dissolved. DIPEA (2.2 mL, 12.9 mmol, 3 eq) and aniline (0.4 mL, 4.29 mmol, 1 eq) were added to the reaction vessel via syringe, stirred at room temperature for 20 min and then irradiated in the microwave at 65°C for 1 h. An additional aliquot of HBTU (1.6 g, 4.29 mmol, 1 eq) was added and irradiated for 1 h at 75°C. Finally, a third addition of HBTU (1.0 g, 4.29 mmol, 1 eq) was made and the reaction was irradiated for 1h at 75°C. The solvent was evaporated in vacuo and the crude product was dissolved in ethyl

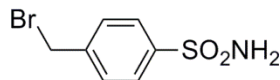
acetate, washed successively with water, sodium bicarbonate solution, and brine. The organic layer was dried over magnesium sulfate, filtered and evaporated to give the crude product which was purified by flash chromatography (15% ethyl acetate/85% hexane). The product containing fractions were combined and the solvent was evaporated to give 473 mg (3.8 mmol, 90%) of the desired compound as a pale yellow solid. $^1\text{H NMR}$ (CDCl_3 , 400 MHz): $\delta = 7.29 - 7.49$ (m, 5H), 4.48 (t, $J = 9.2$, 1H), 3.36 (d, $J = 7.2$, 1H), 2.93 (d, $J = 7.2$, 1H), 1.45 ppm (s, 9H).

α -amino-*N*-phenylsuccinimide·HCl (13)



Compound **12** (500 mg, 1.72 mmol, 1 eq) was combined with 10 mL of 2M HCl in ethanol and the reaction was stirred for 3 hours. The solvent was evaporated in vacuo and the crude product was repeatedly triturated with ethyl acetate to remove impurities. The remaining solid was dried in vacuo to yield 369 mg (1.63 mmol, 95%) of the final product as a pale yellow solid. $^1\text{H NMR}$ (CD_3OD , 400 MHz): $\delta = 7.51$ (t, $J = 8.4$, 3H), 7.40 (d, $J = 7.6$, 2H), 4.36 (t, $J = 9.2$, 1H), 3.21 (d, $J = 9.2$, 1H), 2.93 (d, $J = 6.2$, 1H).

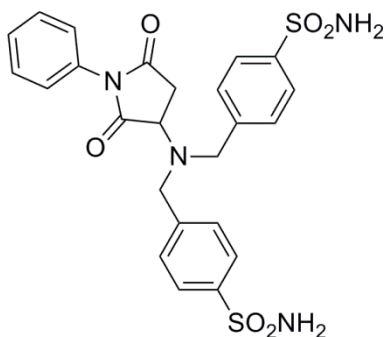
4-(Bromomethyl)benzenesulfonamide (15)



4-(Bromomethyl)benzenesulfonyl chloride (500 mg, 1.86 mmol, 1.0 eq) was dissolved in 10 mL of THF under an argon atmosphere and chilled on ice while stirring. After 10 min, excess 28-30% ammonia (0.5 mL) solution (J.T. Baker) was added dropwise via syringe, the solution was brought to room temperature and then stirred for

another 1.5 h. The reaction mixture was quenched with water and then extracted with ethyl acetate (three times). The combined ethyl acetate extracts were washed with brine (three times), dried over magnesium sulfate, filtered and the solvent was removed in vacuo to give 340 mg (1.36 mmol, 73%) of the final product as a white solid (**86**). ^1H NMR (DMSO- d_6 , 400 MHz): δ = 7.89 (d, J = 8.4, 2H), 7.59 (d, J = 8.4, 2H), 4.61 ppm (s, 2H).

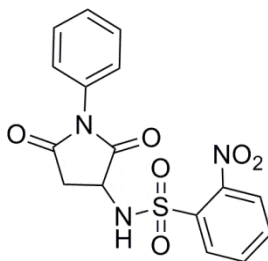
4,4'-(((2,5-dioxo-1-phenylpyrrolidin-3-yl)azanediyl)bis(methylene))dibenzenesulfonamide (16**)**



Fifty milligrams (0.221 mmol, 1 eq) of **13** were dissolved in 8 mL of anhydrous THF in a 20 mL microwave vial. To this, 72 μL of DIPEA (0.442 mmol, 2 eq) was added and the reaction was stirred, under argon at room temperature for 20 min. The solution cleared within 10 min. Compound **15** (82.7 mg, 0.331 mmol, 1.5 eq), dissolved in 2 mL of anhydrous THF was added dropwise to the reaction vial and the reaction was stirred for 30 min at room temperature. The reaction was then irradiated in the microwave for 30 min at 65°C. At this time, 122.3 mg of TBAI (0.331 mmol, 1.5 eq) and 72 μL of DIPEA (0.442 mmol, 2 eq) were added and the solution was again stirred for 30 min at room temperature. Finally, the reaction was sealed and irradiated in the microwave at 65 °C for an additional 30 min. The reaction was dried in vacuo and the crude material was purified by flash chromatography (89% dichloromethane/10% methanol/1% ammonium

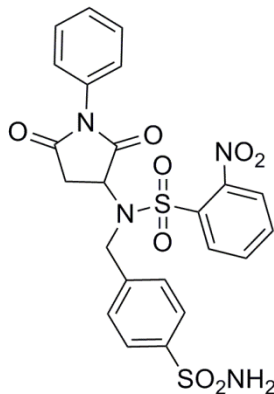
hydroxide) to yield 37.1 mg (0.0702 mmol, 27%) of the product as a white solid. ^1H NMR (CD_3OD , 400 MHz): δ = 7.84 (d, J = 5.6, 4H), 7.60 (d, J = 6.4, 4H), 7.54-7.43 (m, 3H), 7.26 (d, J = 5.6, 2H), 4.17 (t, J = 6.4, 1H), 3.89 (d, J = 6.4, 2H), 3.34 (s, 2H), 3.30 (s, 2H), 2.99 (d, J = 8.4, 1H); MS (TOF-MS, m/z); calculated $[\text{M}+\text{Na}]^+$ for $\text{C}_{24}\text{H}_{24}\text{N}_4\text{O}_6\text{S}_2\text{Na}$ 551.11, found: 551.10.

N-(2,5-dioxo-1-phenylpyrrolidin-3-yl)-2-nitrobenzenesulfonamide (17)



Compound **13** (300 mg, 1.32 mmol, 1eq) was dissolved in 6 mL of dichloromethane (DCM) followed by the addition of DIPEA (1.31 mL, 7.94 mmol, 6 eq). The solution was cooled, while stirring, to 4 °C for 10 min. 4-Nitrobenzenesulfonyl chloride (320 mg, 1.45 mmol, 1.1 eq, 95% pure) was dissolved in 1 mL of DCM and added dropwise to the pre-chilled solution of **13**. During the addition, the solution changed from pale yellow to dark green. The reaction was stirred at room temperature for 24 h under argon atmosphere. At this time, the solvent was evaporated in vacuo. The crude product was semi-purified by flash chromatography (50% ethyl acetate/50% hexane). The resulting semi-pure product was crystallized from chloroform to give **17** (Yield: 150 mg (0.4 mmol, 30%)). ^1H NMR ($\text{DMSO}-d_6$, 400 MHz): δ = 8.42-8.46 (m, 1H), 8.06 (t, J = 7.2, 1H), 7.88 (d, J = 7.6, 2H), 7.47 (t, J = 7.6, 2H), 7.39 (t, J = 7.6, 1H), 7.18 (d, J = 7.6, 2H), 4.88 (t, J = 5.6, 1H), 4.79 (t, J = 5.6, 1H), 3.06 ppm (d, J = 9.6, 1H).

N-(2,5-dioxo-1-phenylpyrrolidin-3-yl)-2-nitro-N-(4-sulfamoylbenzyl)benzenesulfonamide (18)



Compound **17** (56 mg, 0.149 mmol, 1 eq) was dissolved in 1.5 mL of DMF in a 5 mL microwave vessel (Biotage). To this solution, solid cesium carbonate (97.1 mg, 0.298 mmol, 2 eq) was added and the reaction mixture was stirred for 20 min at room temperature. To this, **15** (37.3 mg, 0.149 mmol, 1 eq) was added and the solution was again stirred for 10 min. Finally, the reaction vessel was sealed and irradiated in the microwave for 30 min at 50°C. The solvent was evaporated in vacuo and the product was semi-purified by flash chromatography (70% ethyl acetate/30% hexane). The semi-pure product was finally purified by crystallization from methanol to give **18** (Yield: 20 mg (0.037 mmol, 25%)). ¹H NMR (CD₃OD, 400 MHz): δ = 8.20 (d, *J* = 7.6, 1H), 7.98 (d, *J* = 7.2, 1H) 7.88 (s, *J* = 7.2, 1H), 7.84 (d, *J* = 8.8, 2H), 7.65 (d, *J* = 8.8, 2H), 7.47 (d, *J* = 7.2, 3H), 7.36 (t, *J* = 7.2, 2H), 7.25 (d, *J* = 7.2, 2H), 4.88 (t, *J* = 8.4, 1H), 4.5 (s, 2H), 4.05-4.12 (m, 1H), 3.73 (d, *J* = 8.4, 1H), 3.55 (dd, *J* = 8.4, 1H), 3.05 ppm (d, *J* = 8.4, 1H).

3.4.6 Optical rotation of compounds 11, 12 and 13

Optical rotation of compounds **11**, **12** and **13** were determined by Dr. Shiv Sharma using Perkin-Elmer 241 polarimeter with the cell length of 100 mm. Sodium lamp (589 nm) and Mercury lamp (578 nm) were employed in the polarimetry measurements. Each compound (10 mg) was dissolved in 1.0 mL of HPLC grade

methanol followed by the filtration of this mixture using a micro filter. The standard consisted of pure HPLC grade methanol. Generated data is summarized in the Table 3.4.1

Table 3.4.1 Optical rotation data for L-isomers of compounds **11**, **12**, and **13**.

Compound (L- isomers)	Optical Rotation (α)	
	Mercury lamp	Sodium lamp
11	-5.5	-5.2
12	+4.3	+3.9
13	-15.5	-13.7

REFERENCES

1. Davies, J., and Davies, D. (2010) Origins and evolution of antibiotic resistance, *Microbiology and Molecular Biology Reviews* 74, 417-433.
2. Andersson, D. I., and Hughes, D. (2010) Antibiotic resistance and its cost: is it possible to reverse resistance?, *Nature Reviews Microbiology* 8, 260-271.
3. Wright, G. (2010) Q&A: Antibiotic resistance: where does it come from and what can we do about it?, *BMC biology* 8, 123.
4. Geddes, A. (2008) 80th Anniversary of the discovery of penicillin An appreciation of Sir Alexander Fleming, *International Journal of Antimicrobial Agents* 32, 373.
5. Kohanski, M. A., Dwyer, D. J., and Collins, J. J. (2010) How antibiotics kill bacteria: from targets to networks, *Nature Reviews Microbiology* 8, 423-435.
6. White, R. J. (2012) The Early History of Antibiotic Discovery: Empiricism Ruled, *Antibiotic Discovery and Development*, 3-31.
7. Allen, H. K., Donato, J., Wang, H. H., Cloud-Hansen, K. A., Davies, J., and Handelsman, J. (2010) Call of the wild: antibiotic resistance genes in natural environments, *Nature Reviews Microbiology* 8, 251-259.
8. Cohen, T., Becerra, M. C., and Murray, M. B. (2004) Isoniazid resistance and the future of drug-resistant tuberculosis, *Microbial Drug Resistance* 10, 280-285.
9. Livermore, D. M. (2002) Multiple mechanisms of antimicrobial resistance in *Pseudomonas aeruginosa*: our worst nightmare?, *Clinical Infectious Diseases* 34, 634.
10. Hachem, R. Y., Chemaly, R. F., Ahmar, C. A., Jiang, Y., Boktour, M. R., Rjaili, G. A., Bodey, G. P., and Raad, I. I. (2007) Colistin is effective in treatment of infections caused by multidrug-resistant *Pseudomonas aeruginosa* in cancer patients, *Antimicrobial Agents and Chemotherapy* 51, 1905-1911.

11. Foster, T. J. (2004) The Staphylococcus aureus "superbug", *The Journal of Clinical Investigation* 114, 1693-1696.
12. Hiramatsu, K., Hanaki, H., Ino, T., Yabuta, K., Oguri, T., and Tenover, F. C. (1997) Methicillin-resistant Staphylococcus aureus clinical strain with reduced vancomycin susceptibility, *Journal of Antimicrobial Chemotherapy* 40, 135-136.
13. Hamad, B. (2010) The antibiotics market, *Nature Reviews Drug Discovery* 9, 675-676.
14. Donadio, S., Maffioli, S., Monciardini, P., Sosio, M., and Jabes, D. (2010) Antibiotic discovery in the twenty-first century: current trends and future perspectives, *The Journal of Antibiotics* 63, 423-430.
15. Morel, C. M., and Mossialos, E. (2010) Stoking the antibiotic pipeline, *BMJ* 340.
16. Wright, G. D., and Poinar, H. (2012) Antibiotic resistance is ancient: implications for drug discovery, *Trends in Microbiology* 20, 157-159.
17. Firestine, S. M., Paritala, H., McDonnell, J. E., Thoden, J. B., and Holden, H. M. (2009) Identification of inhibitors of N5-carboxyaminoimidazole ribonucleotide synthetase by high-throughput screening, *Bioorganic & Medicinal Chemistry* 17, 3317-3323.
18. Mathews, I. I., Kappock, T. J., Stubbe, J. A., and Ealick, S. E. (1999) Crystal structure of Escherichia coli PurE, an unusual mutase in the purine biosynthetic pathway, *Structure* 7, 1395-1406.
19. Buchanan, J. M., and Wilson, D. W. (1953) Biosynthesis of purines and pyrimidines, *Federation Proceedings* 12, 646.
20. Zhang, Y., Morar, M., and Ealick, S. E. (2008) Structural biology of the purine biosynthetic pathway, *Cellular and Molecular Life Sciences* 65, 3699-3724.

21. Tranchimand, S., Starks, C. M., Mathews, I. I., Hockings, S. C., and Kappock, T. J. (2011) *Treponema denticola* PurE Is a Bacterial AIR Carboxylase, *Biochemistry* 50, 4623-4637.
22. Murray, A. W. (1971) The biological significance of purine salvage, *Annual Review of Biochemistry* 40, 811-826.
23. An, S., Kumar, R., Sheets, E. D., and Benkovic, S. J. (2008) Reversible compartmentalization of de novo purine biosynthetic complexes in living cells, *Science* 320, 103-106.
24. Galperin, M. Y., and Koonin, E. V. (1997) A diverse superfamily of enzymes with ATP-dependent carboxylate-amine/thiol ligase activity, *Protein Science* 6, 2639-2643.
25. Fawaz, M. V., Topper, M. E., and Firestine, S. M. (2011) The ATP-grasp enzymes, *Bioorganic Chemistry* 39, 185-191.
26. Watanabe, W., Sampei, G., Aiba, A., and Mizobuchi, K. (1989) Identification and sequence analysis of *Escherichia coli* purE and purK genes encoding 5'-phosphoribosyl-5-amino-4-imidazole carboxylase for de novo purine biosynthesis, *Journal of Bacteriology* 171, 198-204.
27. Chen, Z. D., Dixon, J. E., and Zalkin, H. (1990) Cloning of a chicken liver cDNA encoding 5-aminoimidazole ribonucleotide carboxylase and 5-aminoimidazole-4-N-succinocarboxamide ribonucleotide synthetase by functional complementation of *Escherichia coli* pur mutants, *Proceedings of the National Academy of Sciences* 87, 3097.
28. Meyer, E., Leonard, N. J., Bhat, B., Stubbe, J., and Smith, J. M. (1992) Purification and characterization of the purE, purK, and purC gene products:

identification of a previously unrecognized energy requirement in the purine biosynthetic pathway, *Biochemistry* 31, 5022-5032.

29. Mueller, E. J., Meyer, E., Rudolph, J., Davisson, V. J., and Stubbe, J. A. (1994) N5-carboxyaminoimidazole ribonucleotide: evidence for a new intermediate and two new enzymic activities in the de novo purine biosynthetic pathway of *Escherichia coli*, *Biochemistry* 33, 2269-2278.
30. Paritala, H. (2011) Enzymology and medicinal chemistry of N5-carboxyaminoimidazole ribonucleotide synthetase: A novel antibacterial target, Wayne State University.
31. McFarland, W. C., and Stocker, B. A. D. (1987) Effect of different purine auxotrophic mutations on mouse-virulence of a Vi-positive strain of *Salmonella dublin* and of two strains of *Salmonella typhimurium*, *Microbial Pathogenesis* 3, 129-141.
32. Bacon, G. A., Burrows, T. W., and Yates, M. (1951) The effects of biochemical mutation on the virulence of *Bacterium typhosum*: the loss of virulence of certain mutants, *British Journal of Experimental Pathology* 32, 85-96.
33. Kirsch, D. R., and Whitney, R. R. (1991) Pathogenicity of *Candida albicans* auxotrophic mutants in experimental infections, *Infection and Immunity* 59, 3297-3300.
34. Perfect, J. R., Toffaletti, D. L., and Rude, T. H. (1993) The gene encoding phosphoribosylaminoimidazole carboxylase (ADE2) is essential for growth of *Cryptococcus neoformans* in cerebrospinal fluid, *Infection and Immunity* 61, 4446-4451.

35. Cersini, A., Martino, M. C., Martini, I., Rossi, G., and Bernardini, M. L. (2003) Analysis of virulence and inflammatory potential of *Shigella flexneri* purine biosynthesis mutants, *Infection and Immunity* 71, 7002-7013.
36. Lan, L., Cheng, A., Dunman, P. M., Missiakas, D., and He, C. (2010) Golden pigment production and virulence gene expression are affected by metabolisms in *Staphylococcus aureus*, *Journal of Bacteriology* 192, 3068-3077.
37. Polissi, A., Pontiggia, A., Feger, G., Altieri, M., Mottl, H., Ferrari, L., and Simon, D. (1998) Large-Scale Identification of Virulence Genes from *Streptococcus pneumoniae*, *Infection and Immunity* 66, 5620-5629.
38. Samant, S., Lee, H., Ghassemi, M., Chen, J., Cook, J. L., Mankin, A. S., and Neyfakh, A. A. (2008) Nucleotide biosynthesis is critical for growth of bacteria in human blood, *PLoS Pathogens* 4, e37.
39. Thoden, J. B., Holden, H. M., and Firestone, S. M. (2008) Structural Analysis of the Active Site Geometry of N5-Carboxyaminoimidazole Ribonucleotide Synthetase from *Escherichia coli*, *Biochemistry* 47, 13346-13353.
40. Brugarolas, P., Duguid, E. M., Zhang, W., Poor, C. B., and He, C. (2011) Structural and biochemical characterization of N5-carboxyaminoimidazole ribonucleotide synthetase and N5-carboxyaminoimidazole ribonucleotide mutase from *Staphylococcus aureus*, *Acta Crystallographica Section D: Biological Crystallography* 67, 707-715.
41. Ivanovics, G., Marjai, E., and Dobozy, A. (1968) The Growth of Purine Mutants of *Bacillus anthracis* in the Body of the Mouse, *Journal of General Microbiology* 53, 147-162.

42. Mahan, M. J., Mekalanos, J. J., and Slauch, J. M. (1993) Selection of bacterial virulence genes that are specifically induced in host tissues, *Science* 259, 686-688.
43. Donovan, M., Schumuke, J. J., Fonzi, W. A., Bonar, S. L., Gheesling-Mullis, K., Jacob, G. S., Davisson, V. J., and Dotson, S. B. (2001) Virulence of a Phosphoribosylaminoimidazole Carboxylase-Deficient *Candida albicans* Strain in an Immunosuppressed Murine Model of Systemic Candidiasis, *Infection and Immunity* 69, 2542-2548.
44. Lipinski, C. A. (2000) Drug-like properties and the causes of poor solubility and poor permeability, *Journal of Pharmacological and Toxicological Methods* 44, 235-249.
45. Jarrahpour, A., Khalili, D., De Clercq, E., Salmi, C., and Brunel, J. (2007) Synthesis, Antibacterial, Antifungal and Antiviral Activity Evaluation of Some New bis-Schiff Bases of Isatin and Their Derivatives, *Molecules* 12, 1720-1730.
46. Silva, J. F. M., Garden, S. J., and Pinto, A. C. (2001) The chemistry of isatins: a review from 1975 to 1999, *Journal of the Brazilian Chemical Society* 12, 273-324.
47. Verma, M., Pandeya, S. N., Singh, K. N., and Stables, J. P. (2004) Anticonvulsant activity of Schiff bases of isatin derivatives, *Acta Pharmaceutica* 54, 49-56.
48. Aboul-Fadl, T., and Bin-Jubair, F. A. S. (2010) Anti-tubercular activity of isatin derivatives, *International Journal of Pharmaceutical Sciences and Research* 1, 113-126.
49. Chiyanzu, I., Clarkson, C., Smith, P. J., Lehman, J., Gut, J., Rosenthal, P. J., and Chibale, K. (2005) Design, synthesis and anti-plasmodial evaluation in vitro of

- new 4-aminoquinoline isatin derivatives, *Bioorganic & Medicinal Chemistry* 13, 3249-3261.
50. Beraldo, H., and Gambinob, D. (2004) The wide pharmacological versatility of semicarbazones, thiosemicarbazones and their metal complexes, *Mini Reviews in Medicinal Chemistry* 4, 31-39.
 51. Varma, R. S., and Nobles, W. L. (1975) Antiviral, antibacterial, and antifungal activities of isatin-mannich bases, *Journal of Pharmaceutical Sciences* 64, 881-882.
 52. Sridhar, S. K., Saravanan, M., and Ramesh, A. (2001) Synthesis and antibacterial screening of hydrazones, Schiff and Mannich bases of isatin derivatives, *European Journal of Medicinal Chemistry* 36, 615-625.
 53. Bergman, J., Lindstrom, J. O., and Tilstam, U. (1985) The structure and properties of some indolic constituents in *Couroupita guianensis* aubl, *Tetrahedron* 41, 2879-2881.
 54. Guo, Y., and Chen, F. Zhongcaoyao 1986, 17, 8, CA 104: 213068f.
 55. Vine, K. L., Matesic, L., Locke, J. M., Ranson, M., and Skropeta, D. (2009) Cytotoxic and anticancer activities of isatin and its derivatives: a comprehensive review from 2000-2008, *Anti-Cancer Agents in Medicinal Chemistry* 9, 397-414.
 56. Bowes, S., Donnelly, J., Josiah, S., Newman, M., Papadatos, J., Sun, D., and Whitty, A. (2005) Adopting a practical statistical approach for evaluating assay agreement in drug discovery, *Journal of Biomolecular Screening* 10, 508-516.
 57. Gronwald, J. W. (1991) Lipid biosynthesis inhibitors, *Weed Science* 39, 435-449.
 58. Gerth, K., Bedorf, N., Irschik, H., Hofle, G., and Reichenbach, H. (1994) The soraphens: a family of novel antifungal compounds from *Sorangium cellulosum*

- (Myxobacteria). I. Soraphen A1 alpha: fermentation, isolation, biological properties, *The Journal of Antibiotics* 47, 23-31.
59. Shen, Y., Volrath, S. L., Weatherly, S. C., Elich, T. D., and Tong, L. (2004) A mechanism for the potent inhibition of eukaryotic acetyl-coenzyme A carboxylase by soraphen A, a macrocyclic polyketide natural product, *Molecular Cell* 16, 881-891.
60. Li, S. X., Tong, Y. P., Xie, X. C., Wang, Q. H., Zhou, H. N., Han, Y., Zhang, Z. Y., Gao, W., Li, S. G., and Zhang, X. C. (2007) Octameric structure of the human bifunctional enzyme PAICS in purine biosynthesis, *Journal of Molecular Biology* 366, 1603-1614.
61. Copeland, R. A. (2000) Reversible inhibitors, *Enzymes: A Practical Introduction to Structure, Mechanism, and Data Analysis* 8, 266-304.
62. Firestine, S. M. (1995) Biochemical and mechanistic characterization of *Gallus gallus* 5-aminoimidazole ribonucleotide carboxylase, Purdue University.
63. Thoden, J. B., Kappock, T. J., Stubbe, J. A., and Holden, H. M. (1999) Three-dimensional structure of N 5-carboxyaminoimidazole ribonucleotide synthetase: a member of the ATP grasp protein superfamily, *Biochemistry* 38, 15480-15492.
64. Meyer, E., Kappock, T. J., Osuji, C., and Stubbe, J. (1999) Evidence for the Direct Transfer of the Carboxylate of N5-Carboxyaminoimidazole Ribonucleotide (N5-CAIR) To Generate 4-Carboxy-5-aminoimidazole Ribonucleotide Catalyzed by *Escherichia coli* PurE, an N5-CAIR Mutase, *Biochemistry* 38, 3012-3018.
65. Li, X., Zheng, Q. C., Zhang, J. L., and Zhang, H. X. (2011) Theoretical study on the mechanism of rearrangement reaction catalyzed by N5-carboxyaminoimidazole ribonucleotide mutase, *Computational and Theoretical Chemistry* 964, 77-82.

66. Constantine, C. Z., Starks, C. M., Christopher, P., Ransome, A. E., Karpowicz, S. J., Francois, J. A., Goodman, R. A., and Kappock, T. J. (2006) Biochemical and structural studies of N 5-carboxyaminoimidazole ribonucleotide mutase from the acidophilic bacterium *Acetobacter aceti*, *Biochemistry* 45, 8193-8208.
67. Firestine, S. M., Wu, W., Youn, H., and Jo Davisson, V. (2009) Interrogating the mechanism of a tight binding inhibitor of AIR carboxylase, *Bioorganic & Medicinal Chemistry* 17, 794-803.
68. Firestine, S. M., and Davisson, V. J. (1993) A tight binding inhibitor of 5-aminoimidazole ribonucleotide carboxylase, *Journal of Medicinal Chemistry* 36, 3484-3486.
69. Firestine, S. M., Poon, S. W., Mueller, E. J., Stubbe, J. A., and Davisson, V. J. (1994) Reactions Catalyzed by 5-Aminoimidazole Ribonucleotide Carboxylases from *Escherichia coli* and *Gallus gallus*: A Case for Divergent Catalytic Mechanisms, *Biochemistry* 33, 11927-11934.
70. Witiak, D. T., Muhi-Eldeen, Z., Mahishi, N., Sethi, O. P., and Gerald, M. C. (1971) L(S)- and D(R)-3-amino-1-phenylpyrrolidines. Stereoselective antagonists for histamine and acetylcholine receptors in vitro, *Journal of Medicinal Chemistry* 14, 24-30.
71. Spialter, L., and Pappalardo, J. A. (1965) *The acyclic aliphatic tertiary amines*, Macmillan New York.
72. Valot, F., Fache, F., Jacquot, R., Spagnol, M., and Lemaire, M. (1999) Gas-phase selective N-alkylation of amines with alcohols over [gamma]-alumina, *Tetrahedron Letters* 40, 3689-3692.

73. Koh, K., Ben, R. N., and Durst, T. (1993) Reaction of (R)-pantolactone esters of alpha-bromoacids with amines a remarkable synthesis of optically active alpha-amino esters, *Tetrahedron Letters* 34, 4473-4476.
74. Croce, P. D., La Rosa, C., and Ritieni, A. (1988) *The Journal of Chemical Research*, 346.
75. Phanstiel, I., O.; , Wang, Q. X., Powell, D. H., Ospina, M. P., and Leeson, B. A. (1999) Synthesis of Secondary Amines via *N*-(Benzoyloxy)amines and Organoboranes, *Journal of Organic Chemistry* 64, 803.
76. Abdel-Magid, A. F., Maryanoff, C. A., and Carson, K. G. (1990) Reductive amination of aldehydes and ketones by using sodium triacetoxyborohydride, *Tetrahedron Letters* 31, 5595-5598.
77. Abdel-Magid, A. F., Carson, K. G., Harris, B. D., Maryanoff, C. A., and Shah, R. D. (1996) Reductive Amination of Aldehydes and Ketones with Sodium Triacetoxyborohydride. Studies on Direct and Indirect Reductive Amination Procedures¹, *The Journal of Organic Chemistry* 61, 3849-3862.
78. Naganawa, A., Matsui, T., Ima, M., Saito, T., Murota, M., Aratani, Y., Kijima, H., Yamamoto, H., Maruyama, T., Ohuchida, S., Nakai, H., and Toda, M. (2006) Further optimization of sulfonamide analogs as EP1 receptor antagonists: Synthesis and evaluation of bioisosteres for the carboxylic acid group, *Bioorganic & Medicinal Chemistry* 14, 7121-7137.
79. Kan, T., and Fukuyama, T. (2004) New strategies: a highly versatile synthetic method for amines, *Chemical Communications*, 353-359.
80. Cardullo, F., Donati, D., Fusillo, V., Merlo, G., Paio, A., Salaris, M., Solinas, A., and Taddei, M. (2006) Parallel protocol for the selective methylation and alkylation of primary amines, *Journal of Combinatorial Chemistry* 8, 834-840.

81. Cardullo, F., Donati, D., Merlo, G., Paio, A., Salaris, M., and Taddei, M. (2005) Deprotection of o-nitrobenzenesulfonyl (nosyl) derivatives of amines mediated by a solid-supported thiol, *Synlett* **16**, 2996-2998.
82. Firestine, S. M. (1994) Reactions catalyzed by 5-aminoimidazole ribonucleotide carboxylases from *Escherichia coli* and *Gallus gallus*: a case for divergent catalytic mechanisms, *Biochemistry (Easton)* **33**, 11927-11934.
83. Hoskins, A. A., Morar, M., Kappock, T. J., Mathews, I. I., Zaugg, J. B., Barder, T. E., Peng, P., Okamoto, A., Ealick, S. E., and Stubbe, J. (2007) N5-CAIR Mutase: Role of a CO₂ Binding Site and Substrate Movement in Catalysis, *Biochemistry* **46**, 2842-2855.
84. Firestine, S. M. (1995) Biochemical and mechanistic characterization of *Gallus gallus* 5-aminoimidazole ribonucleotide carboxylase, Purdue University.
85. Copeland, R. A. (2005) *Evaluation of enzyme inhibitors in drug discovery: a guide for medicinal chemists and pharmacologists*, Vol. 46, John Wiley and Sons.
86. Naganawa, A., Matsui, T., Ima, M., Saito, T., Murota, M., Aratani, Y., Kijima, H., Yamamoto, H., Maruyama, T., and Ohuchida, S. (2006) Further optimization of sulfonamide analogs as EP1 receptor antagonists: Synthesis and evaluation of bioisosteres for the carboxylic acid group, *Bioorganic & Medicinal Chemistry* **14**, 7121-7137.

ABSTRACT**NOVEL INHIBITORS OF THE BACTERIAL *DE NOVO* PURINE BIOSYNTHESIS ENZYMES, *N*⁵-CARBOXYAMINOIMIDAZOLE RIBONUCLEOTIDE SYNTHETASE AND MUTASE**

by

MARIA V FAWAZ**August 2012****Advisor:** Dr. Steven M. Firestine**Major:** Pharmaceutical Sciences**Degree:** Master of Science

Antibiotic resistance has seen a significant increase during the past decade. The increasing frequency of the drug-resistant bacterial infections has amplified the need for novel antimicrobial agents. *De novo* purine biosynthesis is one area that has great potential for antibacterial drug development because this pathway is different in microorganisms versus humans. The difference in the pathway is centered on the synthesis and utilization of the purine intermediate *N*⁵-carboxy-5-aminoimidazole ribonucleotide (*N*⁵-CAIR). Previous studies have shown that *N*⁵-CAIR is a key intermediate in purine biosynthesis in bacteria, yeast and fungi, but not in humans. *N*⁵-CAIR is synthesized from 5-aminoimidazole ribonucleotide (AIR) by the enzyme *N*⁵-CAIR synthetase and it is utilized by *N*⁵-CAIR mutase to produce the intermediate 4-carboxy-5-aminoimidazole ribonucleotide (CAIR). In our laboratory we explored both enzymes as potential targets for the design of novel *de novo* purine biosynthesis inhibitors. Previous studies suggested that the isatin-based inhibitors were promising low micromolar inhibitors of *N*⁵-CAIR synthetase. Here, the biological verification of the isatin compounds as potential "hits" and their kinetic analysis are presented. The second

project involves the discovery, kinetic evaluation, molecular modeling, and exploratory synthesis of the first known, selective inhibitor of N^5 -CAIR mutase.

.

AUTOBIOGRAPHICAL STATEMENT

MARIA V. FAWAZ

EDUCATION

- 2012 M.S. Pharmaceutical Sciences, Wayne State University, Detroit, Michigan, U.S.A.
2010 B.S. Chemistry (Cum Laude), Wayne State University, Detroit, Michigan, U.S.A.
2008 A.S. Chemistry (Summa cum Laude), Henry Ford Community College, Dearborn, Michigan, U.S.A.
2002 High School Diploma, Physico-Mathematical School #3, Cheboksary, Russia

PROFESSIONAL ASSOCIATIONS

- American Chemical Society, Medicinal Chemistry Division (ACS)
American Association for the Advancement of Science (AAAS)
American Association of Pharmaceutical Scientists (AAPS)

COMMITTEE APPOINTMENTS & AWARDS

- Vice President, American Association of Pharmaceutical Scientists, Student Chapter, 2011 (September) - 2012 (May)
Student Representative, College of Pharmacy & Health Sciences Research Committee, 2011- 2012
Eli Lilly/WCC Travel Grant Award, American Chemical Society, 2011
Travel Award, Wayne State University College of Pharmacy & Health Sciences, 2011
Presidential Scholarship, Wayne State University, 2008-2010
Dean's List, Wayne State University, Department of Chemistry, 2009-2010
Departmental Honors Program, Chemistry, Wayne State University, 2008-2010
Stephen Brandt Memorial Scholarship, Henry Ford Community College, 2007-2008
Henry Ford II Honors Program, Henry Ford Community College, 2006-2008

PUBLICATIONS

Fawaz, M.V., Topper, M., Firestine, S. M. (2011). ATP-grasp enzymes. *Bioorganic Chemistry* 39, 185-91.

Topper, M., Sharma, S., Fawaz, M.V., Firestine, S. M. Isatin-based inhibitors of N^5 -carboxyaminoimidazole ribonucleotide synthetase (*manuscript in preparation*).

PRESENTATIONS

Fawaz, M.V., Firestine, S. M. Selective inhibitor of N^5 -carboxyaminoimidazole ribonucleotide mutase: biological evaluation and molecular modeling analysis. 243rd American Chemical Society National Meeting, San Diego, March 25, 2012.

Fawaz, M.V., Firestine, S. M. Selective inhibitor of N^5 -carboxyaminoimidazole ribonucleotide mutase: biological evaluation and molecular modeling analysis. Midwest Enzyme Conference, University of Chicago, October 15, 2011.

Fawaz, M.V., Firestine, S. M. A novel, selective inhibitor of N^5 -carboxyaminoimidazole ribonucleotide mutase. 6th Annual Chemistry-Biology Interface Training Program Symposium, University of Michigan, March 11, 2011.